nature portfolio

Peer Review File

Dynamic construction of durable epitaxial catalytic layer for industrial alkaline water splitting

Corresponding Author: Professor Huabin Zhang

This file contains all reviewer reports in order by version, followed by all author rebuttals in order by version.

Version 0:

Reviewer comments:

Reviewer #1

(Remarks to the Author)
In this manuscript, the authors fabricated nickel molybdate with an epitaxial layer (e-$NiMoO_4$) through the conversion of $NiMoO_4$ via cathodic electrochemical synthesis. The e-$NiMoO_4$ demonstrated good HER activity and was successfully applied as an electrode material for the industrial alkaline electrolyzer.
Based on electrochemical measurements, XPS, XAS analyses, and DFT calculations, it was shown that the structural relaxation induced by molybdenum dissolution under bias is mitigated by the epitaxial hydroxide layer, which provides protection against the structural collapse typically triggered by molybdenum dissolution. The locally enhanced electric field on the dendritic epitaxial catalytic layer increases the concentration of hydrated potassium ions, optimizing the rigid hydrogen-bond network at the interface and further accelerating HER reaction kinetics.
Through XAS analysis, in-situ XAFS, DFT calculations, and MD simulations, the authors not only performed a detailed analysis of the catalyst but also successfully applied it to the industrial alkaline electrolyzer, representing the novelty of this manuscript.
However, clearer structural and compositional characterization of $NiMoO_4$ with surface $Ni(OH)_2$, along with further discussion, are required. This manuscript should be improved by addressing the comments below.

Comment 1: The authors should provide clearer structural, morphological, and compositional characterization of the $NiMoO_4$ part and surface $Ni(OH)_2$, including EDS elemental mapping, line scanning, and compositional analysis, to accurately identify the surface locations of $Ni(OH)_2$. This will help clarify the presentation of the epitaxial hydroxide layer on the surface and support the morphological descriptions provided in Fig. 1.

Comment 2: The optimized cathodic electrochemical synthesis conditions were applied to a 1.5 cm × 1.5 cm electrode. Due to the varying working electrode areas, the current bias differs for larger-sized materials, which can lead to different morphological characteristics in the resulting samples. To address this issue, the authors should provide compositional analysis with EDS elemental mapping for larger-sized e-$NiMoO_4$.

Comment 3: The formation of the surface epitaxial hydroxide layer may influence the d-spacing of the original core $NiMoO_4$ structure. As shown in Fig. S3, a slight shift in the XRD pattern for e-$NiMoO_4$ was observed. It is essential to clearly explain this XRD peak shift. Additionally, the XRD reference for $NiMoO_4$ should be provided.

Comment 4: The XPS and XAS analysis results highlight the improved activity and stability due to the prevention of Mo dissolution during HER and the contribution of surface $Ni(OH)_2$. However, direct experimental evidence is still needed. For instance, are there any structural or crystalline changes in $Ni(OH)_2$ after the HER process? These changes could be influenced not only by the HER reaction under cathodic potential but also by possible re-deposition effects on e-$NiMoO_4$ under cathodic potential in the same alkaline environment.

Comment 5: Please clearly specify the components of the deconvoluted XPS peaks. The explanation regarding surface analysis is insufficient. Since XPS is the most suitable technique for analyzing the surface $Ni(OH)_2$, it needs to be discussed in detail (Fig. S14).

• The slight shift in the XPS O 1s peak is observed in both samples. How is this related to alkaline HER for $NiMoO_4$ and e-$NiMoO_4$?

• In $NiMoO_4$, the Mo XPS peak almost disappears, likely due to Mo dissolution (as described in the manuscript). In contrast, e-$NiMoO_4$ shows a negative shift in both Ni and Mo XPS peaks, along with an increased oxidation state for Mo. This should be explained. As shown in Fig. 3j, there is some question about the claim that Mo in e-$NiMoO_4$ does not participate in any reaction.

• In the Ni 2p XPS region of e-$NiMoO_4$, a Nix peak (around 857 eV) is observed, which weakens after the HER process. This XPS peak is absent in the $NiMoO_4$. Please provide further explanation regarding this.

Comment 6: During electrochemical analysis, is there any activation observed during LSV cycles or CV cycles? Surface reconstruction could occur due to redox reactions under cathodic potential simultaneously with HER.

Comment 7: The epitaxial hydroxide layer on the surface may have affected the ECSA. It would be beneficial to compare the ECSA of the e-$NiMoO_4$-1 or $NiMoO_4$-a, where the epitaxial hydroxide layer is minimally formed, with that of the optimized e-$NiMoO_4$ to demonstrate this effect.

Comment 8: I recommend performing ICP analysis of the electrolyte to provide evidence of Mo dissolution for e-$NiMoO_4$ and $NiMoO_4$.

Reviewer #2

(Remarks to the Author)
Alkaline electrolyzers are currently the most widely adopted technology for large-scale industrial hydrogen production. In this study, Chang and his colleagues investigated the challenges related to the Volmer step of the alkaline water dissociation reaction, as well as the slow kinetics caused by the subsequent desorption of OH* species. Unlike the conventional focus on optimizing the chemical and electronic structures of catalysts, their research centered on the often-overlooked structure of the EDL within the electrolyte. By synchronizing the regulation and optimization of the catalyst-electrolyte interface active sites and the EDL structure, their study gained valuable insights. They demonstrated that the dynamically constructed epitaxial hydroxide layer serves as a protective barrier against molybdenum leaching, significantly enhancing material stability. The dendritic epitaxial layer also intensified the local electric field, optimizing the electrochemical environment at the catalyst-electrolyte interface and thereby accelerating reaction kinetics. Most notably, the optimized material exhibited excellent activity and stability when directly evaluated within an industrial assessment system. This comprehensive study unveiled intriguing experimental phenomena and was thoroughly supported by data analysis, elucidating the complexities of the reaction mechanism and its potential applications in industrial systems. After careful review, I would like to recommend its acceptance in Nature Communications after revision. The following suggestions are provided for the authors:

1. The authors primarily focused on the changes in the coordination structure of nickel during material structural analysis. To strengthen this analysis, it is recommended to include XAFS analysis of Mo in both NiMoO4 and e-NiMoO4 structures, as well as their post-reaction states. This will help to emphasize the structural advantages of e-NiMoO4.

2. The synthesis time and voltage in electrochemical processes are two critical factors. It is suggested to conduct electrochemical analysis on samples with varying reconstruction times. Additionally, incorporating a synthesis schematic would provide a clearer understanding of the synthesis mechanism

3. Based on findings from in-situ XAFS tests, it was observed that the control sample NiMoO4 underwent significant structural collapse and transformation into hydroxides after prolonged cycling, whereas e-NiMoO4 did not exhibit these changes. Including relevant characterization data would offer a more direct visualization of the morphological changes in the two samples post-cycling.

4. The electrochemical results presented in this manuscript indicate a clear trend: as the catalytic activity of $NiMoO_4$ samples improves, there is a corresponding decrease in the Tafel slope. This relationship remains consistent even when varying both the reconstruction potential and reconstruction time (as shown in Supplementary Fig. 10 and 26). Given that the Tafel slope provides significant insights into the rate-determining step and reaction mechanism in the HER, rather than merely describing catalytic performance, it is essential for the authors to provide a more comprehensive discussion of the underlying mechanistic implications based on the electrochemical data.

5. Regarding the DFT models, it is crucial to verify whether a k-point optimization was performed. The impact of low-coordination oxygen atoms on the Fermi level in the lower slab should also be considered. Moreover, the authors should investigate how the introduction of K+ influences surface adsorption energy and reaction pathways during modeling.

Reviewer #3

(Remarks to the Author)
Report: Dynamic construction of durable epitaxial catalytic layer for industrial alkaline water splitting

The goal of the authors is to introduce a dual-optimization strategy of dynamically constructing an epitaxial catalytic layer.

The subject of the submitted paper carried out an interesting issue related to hydrogen production.
Please find the attached file, which highlights in yellow or red color some possible misspellings or little grammatical suggestions.
My principal concern is related to the computational issue.

1. The introduction section contains many short sentences with many references. I suggest citing review papers and, additionally, discussing the results with data from the literature. For example, reference number 18 should be discussed in the results section instead of being cited in a generic paragraph in the introduction;
2. I am confident that synergy between experiment and theory is an important branch of research. However, both approaches must be discussed at the same high level, and the lack of information can make it difficult to interpret or reproduce both observations and, consequently, the correlation between both results and observation. Perhaps some computational details of information can be added to the supplementary material.
i) The theoretical model does not show the symmetry used in the computational models, nor does it describe which surface direction of NiMoO4 is related to the morphology shown in the micrographs. For example, see Figure 1;
ii) Where is the adopted crystallographic information file (CIF) file?
iii) The calculation of Gibbs free energies is not clearly explained. Did harmonic calculation calculate it? How to obtain the TS parameter?
iv) Please, the DFT computational details section should be moved out of the characterization section.
v) What is the state of the art on NiMoO4?
vi) A lack of references has been noticed throughout the work. Among them, COMSOL and more….
vii) Where is the CIF file for each adopted model?
viii) The total and projected density of states does not bring relevant pieces of information. I suggest COHP analysis and a more detailed discussion :
https://pubs.acs.org/doi/10.1021/jp202489s
3. The water-splitting mechanism and hydrogen evolution reaction deserve to be elucidated. Much of this can be extracted by quantum mechanical methods.

Version 1:

Reviewer comments:

Reviewer #1

(Remarks to the Author)
The revisions and additional experimental data provided have significantly strengthened your manuscript. The clarification of the fundamental mechanisms, along with the refined discussion on catalyst stability and performance, have addressed the initial concerns effectively.

Considering the substantial improvements made, I believe the manuscript is now well-prepared for publication in Nature Communications.

Reviewer #2

(Remarks to the Author)
The authors carefully addressed my technical concerns. The manuscript can be published as is.

Reviewer #3

(Remarks to the Author)
Dear Edidor,

I carefully read the referee's response, and I believe the manuscript has been improved.
I think that the manuscript will be able to the readers of Nature communications

Point-by-point Response to Review Comments

We express our gratitude to the editor and reviewers for their comprehensive evaluation and providing valuable comments and suggestions, which significantly enhances the quality and clarity of our manuscript and have also provided important guidance for our future work. We have carefully consider all the reviewer suggestion and comments in the revised manuscript. We also provided the corresponding responses as follows.

Reviewers' comments and our Response:

Reviewer #1 (Comments to the Author): ==========

In this manuscript, the authors fabricated nickel molybdate with an epitaxial layer (e-$NiMoO_4$) through the conversion of $NiMoO_4$ via cathodic electrochemical synthesis. The e-$NiMoO_4$ demonstrated good HER activity and was successfully applied as an electrode material for the industrial alkaline electrolyzer. Based on electrochemical measurements, XPS, XAS analyses, and DFT calculations, it was shown that the structural relaxation induced by molybdenum dissolution under bias is mitigated by the epitaxial hydroxide layer, which provides protection against the structural collapse typically triggered by molybdenum dissolution. The locally enhanced electric field on the dendritic epitaxial catalytic layer increases the concentration of hydrated potassium ions, optimizing the rigid hydrogen-bond network at the interface and further accelerating HER reaction kinetics. Through XAS analysis, in-situ XAFS, DFT calculations, and MD simulations, the authors not only performed a detailed analysis of the catalyst but also successfully applied it to the industrial alkaline electrolyzer, representing the novelty of this manuscript. However, clearer structural and compositional characterization of $NiMoO_4$ with surface $Ni(OH)_2$, along with further discussion, are required. This manuscript should be improved by addressing the comments below.

Our response: We sincerely appreciate your recognition and encouraging comments on manuscript. We carefully considered all comments and provided a point-by-point response as outlined below:

Specific comments:

Q1: *The authors should provide clearer structural, morphological, and compositional characterization of the $NiMoO_4$ part and surface $Ni(OH)_2$, including EDS elemental mapping,*

line scanning, and compositional analysis, to accurately identify the surface locations of $Ni(OH)_2$. This will help clarify the presentation of the epitaxial hydroxide layer on the surface and support the morphological descriptions provided in Fig. 1.

Our response: We sincerely appreciate your insightful suggestions. In response to the request for enhanced characterization of the $NiMoO_4$ structure and surface $Ni(OH)_2$ layer, we have performed additional experiments and analyses, including EDS elemental mapping, cross-sectional line scanning, and surface compositional analysis, to clarify the spatial distribution and chemical states of Ni, Mo, and O in both the bulk and surface regions. Low-magnification EDS mapping confirms the uniform distribution of Ni, Mo, and O within the bulk material (Supplementary **Fig. 5a**). Cross-sectional line scanning at the interface reveals a pronounced surface enrichment of Ni relative to Mo, consistent with the epitaxial growth of the $Ni(OH)_2$ layer on the $NiMoO_4$ substrate. TEM mapping at different magnifications, along with aberration-corrected mapping, clearly demonstrates the epitaxial relationship between the $NiMoO_4$ core and the $Ni(OH)_2$ shell (Supplementary **Fig.4** and **5b-c**). Lattice fringes further validate the structural coherence at the interface. These findings highlight the spatial and compositional distinction between $NiMoO_4$ and $Ni(OH)_2$, providing strong evidence for the proposed surface hydroxide layer formation and its epitaxial growth mechanism. The newly supplemented data are summarized below and have been added to the revised manuscript:

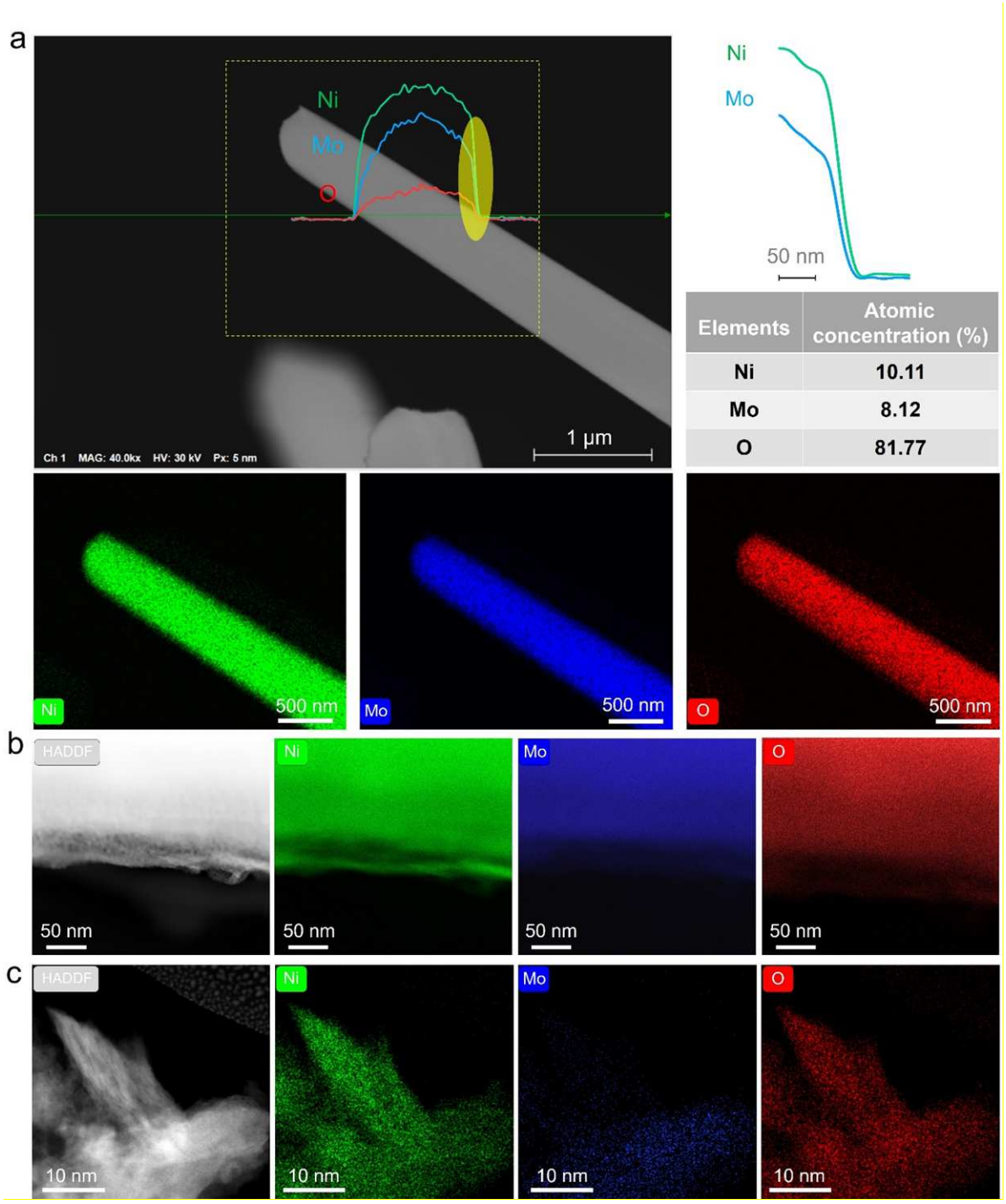

Supplementary Fig. 5 a, EDS elemental mapping with cross-sectional line scanning. **b**, HRTEM elemental mapping. **c**, HAADF- STEM elemental mapping.

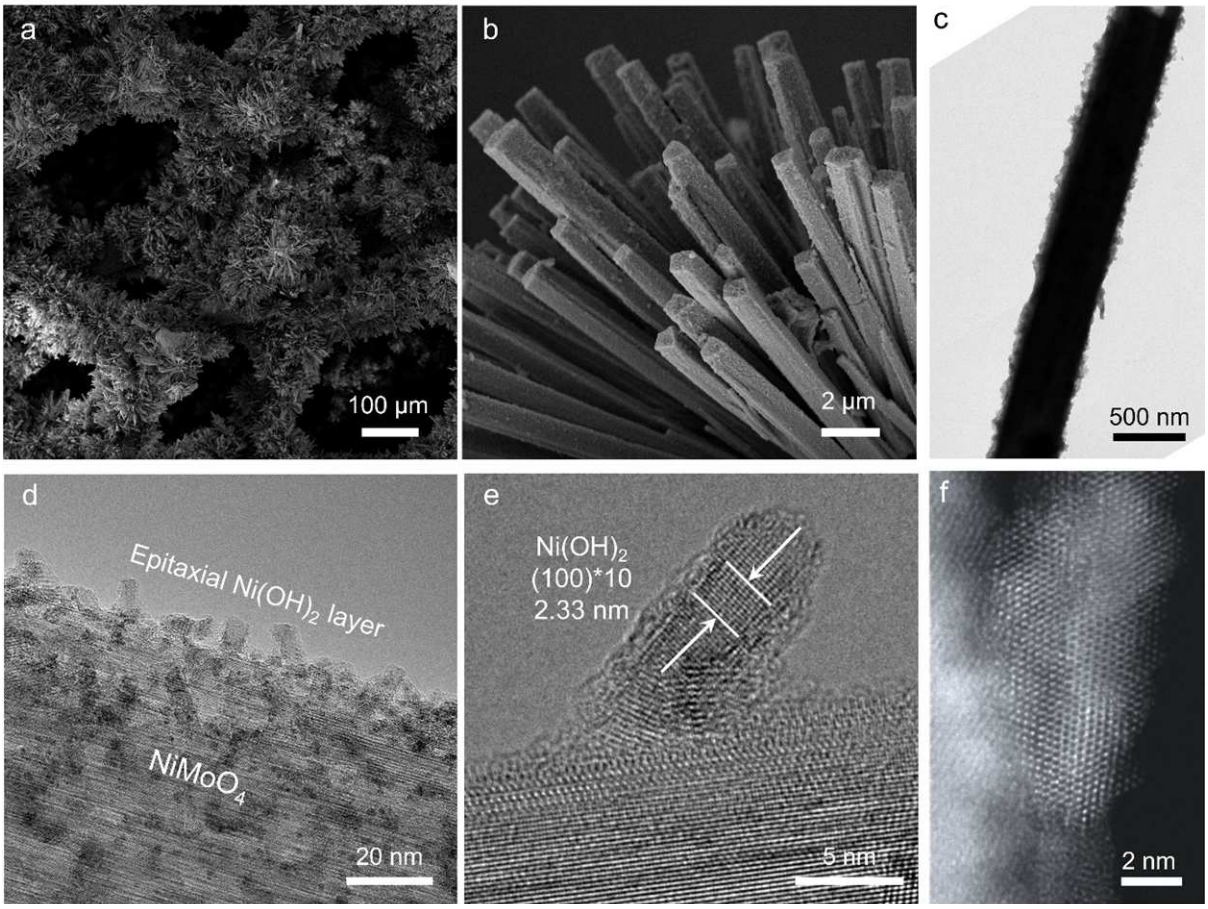

Supplementary Fig. 4 a, b, SEM image of e-$NiMoO_4$ at different magnification. **c,** TEM image of e-$NiMoO_4$. **d, e,** HRTEM image of e-$NiMoO_4$ at different magnification. **f,** High-resolution HAADFSTEM image of e-$NiMoO_4$.

"SEM elemental mapping confirms the uniform distribution of Ni, Mo, and O (Supplementary Fig. 5a). Additionally, STEM mapping at various magnifications, including aberration-corrected imaging, clearly illustrates the epitaxial relationship between the $NiMoO_4$ core and the $Ni(OH)_2$ shell (Supplementary Fig. 5b-c)."***(Page 5 in revised manuscript)***

Q2: *The optimized cathodic electrochemical synthesis conditions were applied to a 1.5 cm × 1.5 cm electrode. Due to the varying working electrode areas, the current bias differs for larger-sized materials, which can lead to different morphological characteristics in the resulting samples. To address this issue, the authors should provide compositional analysis with EDS elemental mapping for larger-sized e-*$NiMoO_4$*.*

Our response: Thank you for raising this critical point on the scalability of the synthesis process. To rigorously address the potential impact of electrode size on material uniformity,

we have conducted additional compositional and morphological analyses on the e-$NiMoO_4$ electrode with different larger size of 3 × 3 cm, 6 × 6 cm and 6 × 20 cm. As noted by the reviewer, the current varies among electrode sheets of different sizes under the same reconstruction voltage, directly influencing the reconstruction process (Figure **R1**). To address this, the precursor material composition was optimized to ensure that SEM images of electrodes of all sizes exhibited a nanorod morphology consistent with that of the original small-sized samples (Figure 1). Additionally, strict control of current density was implemented by proportionally adjusting the total current using a DC power source, ensuring a uniform current density of 200 mA/cm^2 across all electrode sizes and preventing localized overpotential effects. For large-scale electrode reconstruction systems, dynamic electrolyte flow was regulated using a peristaltic pump-driven circulation system to mitigate mass transport limitations, minimize concentration polarization, and maintain temperature stability, thereby ensuring uniform ion distribution and local pH during reconstruction. Transmission electron microscopy confirmed that the optimized reconstructed electrodes of different sizes retained a surface dendritic layer, demonstrating that current density control effectively preserved the nanostructure during scale-up (Supplementary **Fig. 12-13**). EDS mapping further verified the homogeneous spatial distribution of Ni, Mo, and O across samples of varying sizes (Supplementary **Fig. 14**). The corresponding synthesis procedures and newly supplemented data have been incorporated into the revised manuscript and supporting information:

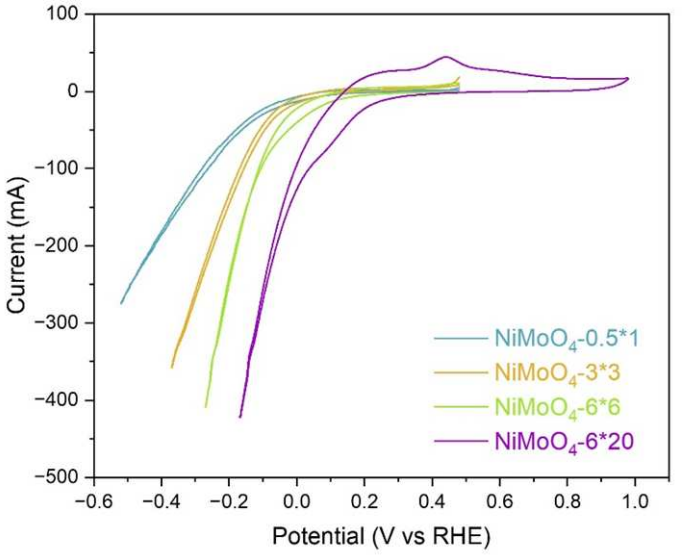

Fig. R1 Cyclic voltammetry curves of electrode with different sizes.

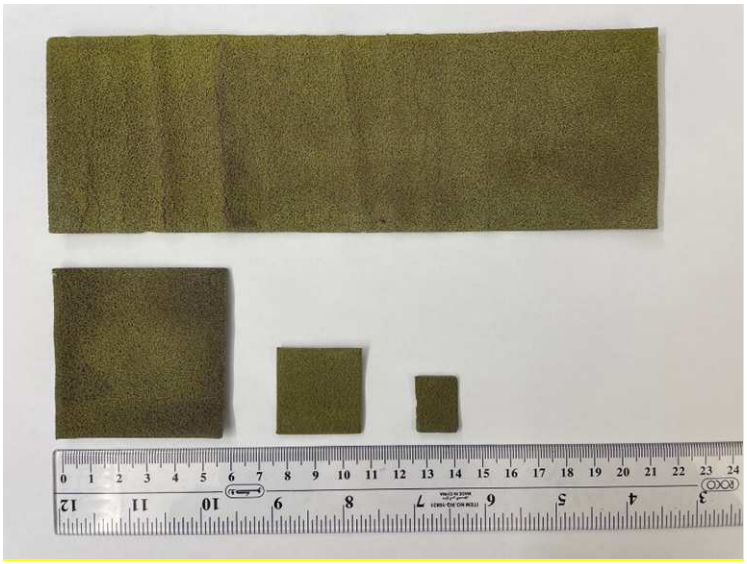

Supplementary Fig. 12 Photograph of e-$NiMoO_4$ electrode with different sizes.

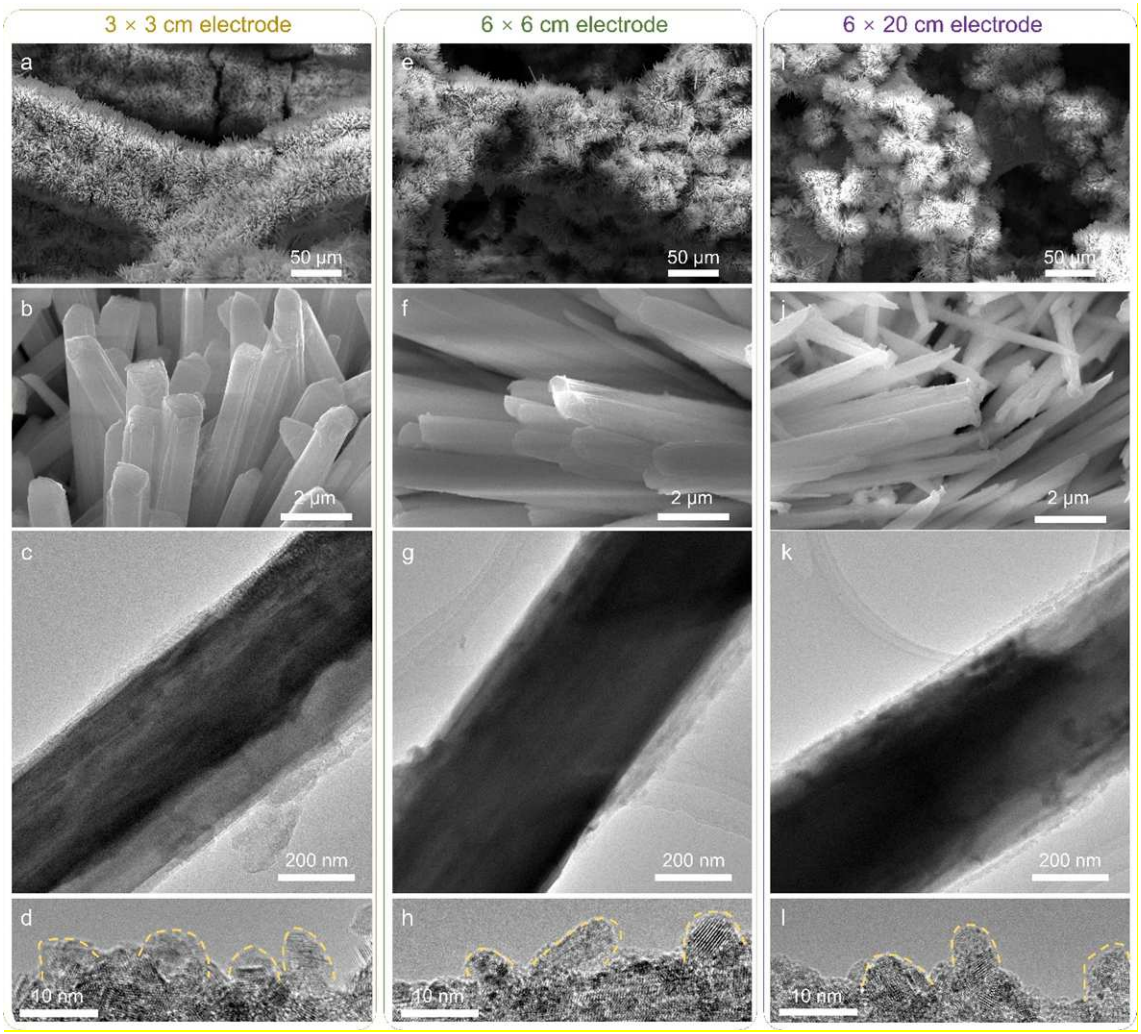

Supplementary Fig. 13 a, b, e, f, i, j SEM images of e-$NiMoO_4$ with different sizes at different magnifications. **c, d, g, h, k, l** TEM images of e-$NiMoO_4$ with different sizes at different

magnifications.

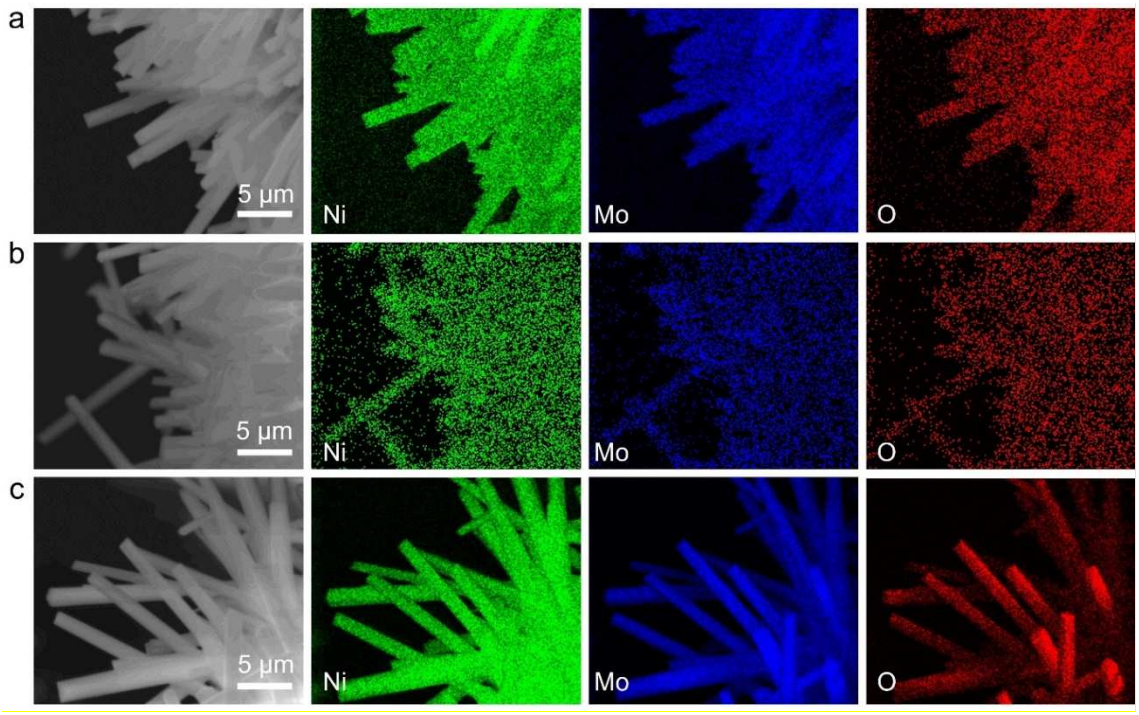

Supplementary Fig. 14 EDS-mapping images of e-$NiMoO_4$ with different sizes (**a,** 3 × 3 cm, **b,** 6 × 6 cm and **c,** 6 × 20 cm)

"The current density was precisely controlled by proportionally adjusting the total current using a DC power supply. A uniform current density of 200 mA/cm² was maintained across all electrode sizes to prevent localized overpotential effects[4]. For large-scale electrode reconstruction systems, a peristaltic pump-driven circulation system was employed to regulate dynamic electrolyte flow, mitigating mass transport limitations, minimizing concentration polarization, and maintaining temperature stability. This approach ensured uniform ion distribution and local pH stability during the reconstruction process, ultimately enabling the optimized synthesis of electrodes with various sizes."***(Page 13 in revised supplementary materials)***

"For the electrochemical synthesis of large-scale electrodes, a DC power supply (Maisheng KKS605N, 0~60V, 0~5A) equipped with a peristaltic pump-driven circulation system was employed under ambient temperature and pressure. The current was maintained at 200 mA/cm², and the synthesis duration was kept consistent with that of smaller electrodes."***(Page 15 in revised manuscript)***

Supplementary Reference:

4. Meharban F., *et al.* Scaling up stability: Navigating from lab insights to robust oxygen evolution electrocatalysts for industrial water electrolysis. *Adv. Energy Mater.* **14**, (2024).

Q3: *The formation of the surface epitaxial hydroxide layer may influence the d-spacing of the original core $NiMoO_4$ structure. As shown in Fig. S3, a slight shift in the XRD pattern for e-$NiMoO_4$ was observed. It is essential to clearly explain this XRD peak shift. Additionally, the XRD reference for $NiMoO_4$ should be provided.*

Our response: We sincerely appreciate your valuable comments. We agree that the formation of an epitaxial hydroxide layer on the surface may influence the *d*-spacing of the original $NiMoO_4$ core structure, leading to a shift in the XRD peak positions. This shift primarily results from changes in the lattice parameters induced by the growth of the surface hydroxide layer. As the hydroxide layer epitaxially grows on the $NiMoO_4$ surface, the newly formed interface generates stress, which propagates into the $NiMoO_4$ lattice, causing slight lattice expansion and distortion. Consequently, this alteration in *d*-spacing manifests as a negative peak shift in the XRD pattern (Supplementary **Fig. 3**). The corresponding newly supplemented data have been incorporated into the revised manuscript and supporting information:

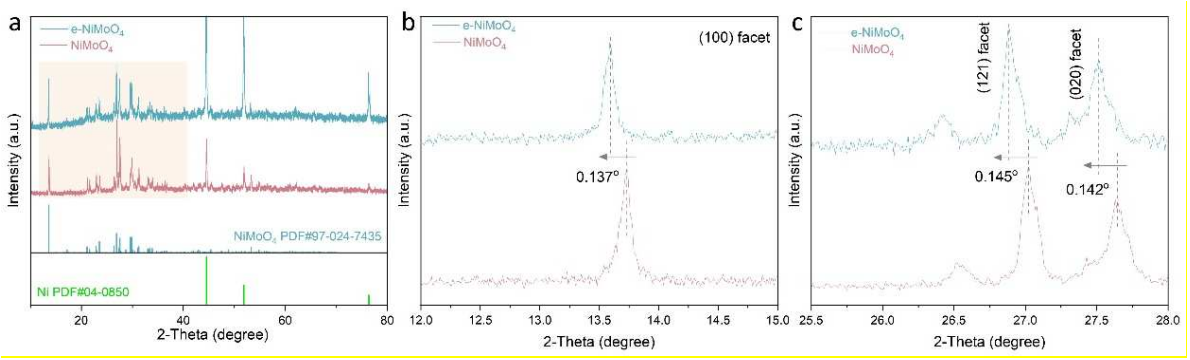

Supplementary Fig. 3 a, XRD patterns of e-$NiMoO_4$ and $NiMoO_4$. **b, c,** The corresponding enlarged area of XRD patterns.

"During the epitaxial growth of the hydroxide layer on the $NiMoO_4$ surface, the newly formed interface generates stress, which propagates into the $NiMoO_4$ lattice, causing slight lattice expansion and distortion. Consequently, the formation of the surface hydroxide layer may alter the d-spacing of the original $NiMoO_4$ core structure, leading to a negative shift in the XRD peak positions[1, 2]."***(Page 4 in revised supplementary materials)***

Supplementary Reference:

1. Solomon G., *et al.* $NiMoO_4@Co_3O_4$ core–shell nanorods: In situ catalyst reconstruction toward high efficiency oxygen evolution reaction. *Adv. Energy Mater.* **11**, (2021).
2. Jiang R., *et al.* Redox promoted rapid and deep reconstruction of defect-rich nickel precatalysts for efficient water oxidation. *Small* **20**, e2401384 (2024).

Q4: *The XPS and XAS analysis results highlight the improved activity and stability due to the prevention of Mo dissolution during HER and the contribution of surface* $Ni(OH)_2$*. However, direct experimental evidence is still needed. For instance, are there any structural or crystalline changes in* $Ni(OH)_2$ *after the HER process? These changes could be influenced not only by the HER reaction under cathodic potential but also by possible re-deposition effects on e-*$NiMoO_4$ *under cathodic potential in the same alkaline environment.*

Our response: Thanks for your critical comments. To evaluate the stability of $Ni(OH)_2$ and its potential dissolution-redeposition behavior, we subjected both e-$NiMoO_4$ and $NiMoO_4$ to HER conditions (-0.2 V vs. RHE) in 1.0 M KOH (free of nickel and molybdenum precursors) for 10 hours. TEM analysis revealed that the surface of $NiMoO_4$ was covered by a thick layer of $Ni(OH)_2$ nanosheets, whereas the $Ni(OH)_2$ dendritic layer on e-$NiMoO_4$ remained largely intact, with only minor particle aggregation (Supplementary **Fig. 21-22**). Subsequent ICP analysis confirmed the dissolution of Ni and Mo in the $NiMoO_4$ system (Ni: 0.12 ppm, Mo: 7.08 ppm), while their dissolution in the e-$NiMoO_4$ system was significantly suppressed (Ni: 0.09 ppm, Mo: 0.85 ppm) (Supplementary **Table 2**). Furthermore, cyclic voltammetry (CV) cycling tests on e-$NiMoO_4$ showed a slight initial increase in electrode activity after the first 10 cycles, which can be attributed to improved electrode wettability (Supplementary **Fig. 20**). After 100 cycles, the material maintained stable activity without the emergence of significant redox peaks, ruling out substantial redeposition of dissolved species. The newly supplemented data are summarized below and have been added to the revised manuscript:

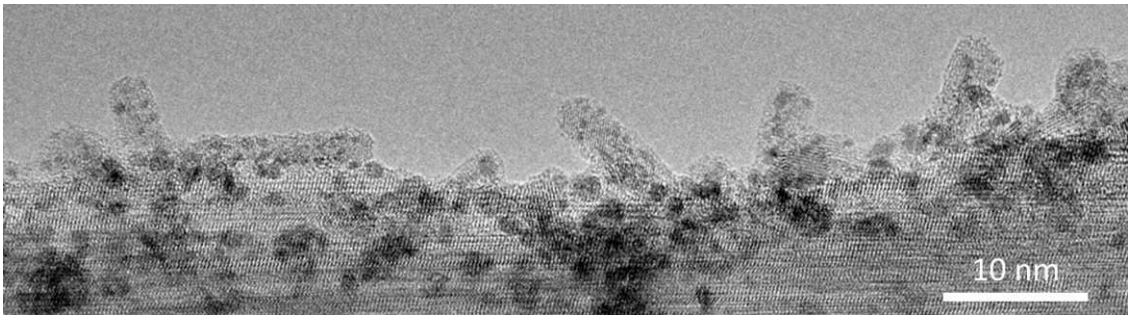

Supplementary Fig. 21 TEM image of e-$NiMoO_4$ after reaction.

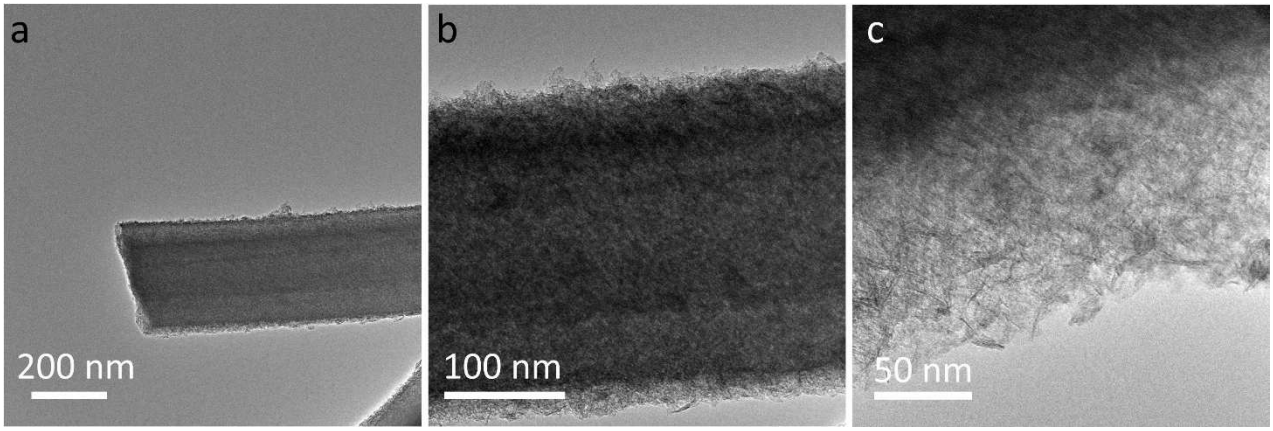

Supplementary Fig. 22 a, b, c, TEM image of e-$NiMoO_4$ after reaction at different magnifications.

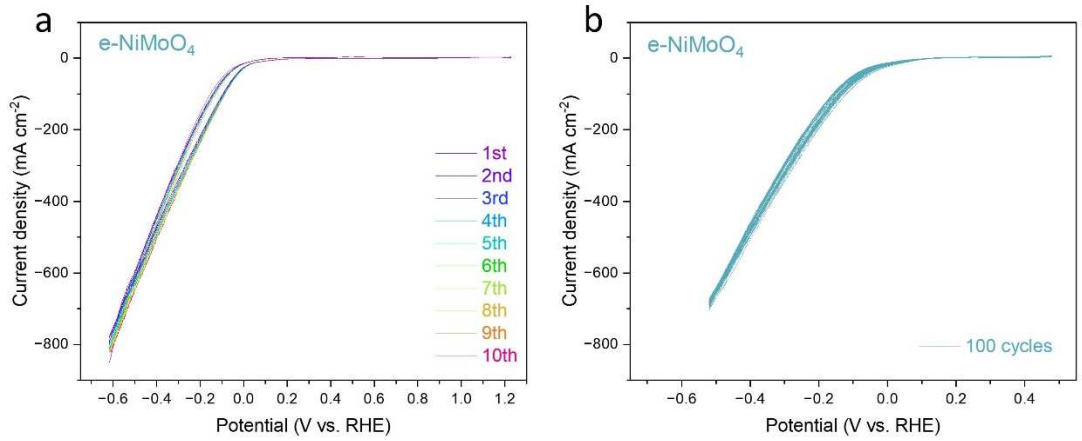

Supplementary Fig. 20 a, Cyclic voltammetry curves of the first ten cycles. **b,** Cyclic voltammetry curves for 100 cycles.

Supplementary Table 2. The ICP analysis of metal dissolution behavior under both natural and operational conditions.

Testing Conditions	Electrode Soaking (10 h)		HER Reaction (10 h)	
Materials	$NiMoO_4$	e-$NiMoO_4$	$NiMoO_4$	e-$NiMoO_4$
Dissolved Ni (ppm)	0.31	0.11	0.12	0.09
Dissolved Mo (ppm)	14.0	1.89	7.08	0.85

"TEM analysis revealed that a thick layer of $Ni(OH)_2$ nanosheets formed on the $NiMoO_4$ surface, whereas the $Ni(OH)_2$ dendritic layer on e-$NiMoO_4$ remained largely intact, with only

minor particle aggregation (Supplementary Fig. 21-22). Subsequent ICP analysis confirmed the dissolution of Ni and Mo in the $NiMoO_4$ system (Ni: 0.12 ppm, Mo: 7.08 ppm), while their dissolution in the e-$NiMoO_4$ system was significantly suppressed (Ni: 0.09 ppm, Mo: 0.85 ppm) (Supplementary Table 2)."***(Page 8 in revised manuscript)***

"Cyclic voltammetry (CV) cycling tests indicate a slight increase in current density after the first 10 cycles, which can be attributed to improved electrode wettability[6]. After 100 cycles, the material maintains stable activity without noticeable redox peaks, ruling out significant redeposition of dissolved species."***(Page 23 in revised supplementary materials)***

"e-$NiMoO_4$ and $NiMoO_4$ were subjected to HER conditions (-0.2 V vs. RHE) in 1.0 M KOH for 10 hours. A thick layer of $Ni(OH)_2$ nanosheets formed on the $NiMoO_4$ surface, whereas the $Ni(OH)_2$ dendritic layer on e-$NiMoO_4$ remained largely intact, with only minor particle aggregation."***(Pages 24 in revised supplementary materials)***

Supplementary Reference:

6. Liang Y., Han Y., Li J.-s., Wang J., Liu D., Fan Q. Wettability control in electrocatalyst: A mini review. *J. Energy Chem.* **70**, 643-655 (2022).

Q5: *Please clearly specify the components of the deconvoluted XPS peaks. The explanation regarding surface analysis is insufficient. Since XPS is the most suitable technique for analyzing the surface $Ni(OH)_2$, it needs to be discussed in detail (Fig. S14).*

Our response: Thanks for your valuable suggestions on refining our analysis of the material's surface structure. Regarding the deconvoluted XPS peaks, we have conducted a detailed assignment and analysis during the original data processing. In the revised manuscript, we will provide comprehensive annotations in the supplementary materials to clearly indicate the composition corresponding to each deconvoluted peak (Supplementary **Fig. 6** and **23**). For the Ni 2p peaks, we primarily include the Ni^{2+} $2p_{3/2}$ and $2p_{1/2}$ peaks, along with their associated satellite peaks. The Mo 3d peaks consist of Mo $3d_{5/2}$ and $3d_{3/2}$ components. The O 1s peak, after deconvolution, can be classified into different components, including lattice oxygen (coordinated with Ni and Mo) and surface hydroxyl oxygen. We have provided detailed explanations in the figure captions and supplementary text regarding the origin of each component and its corresponding binding energy range to enhance the clarity and readability of the manuscript.

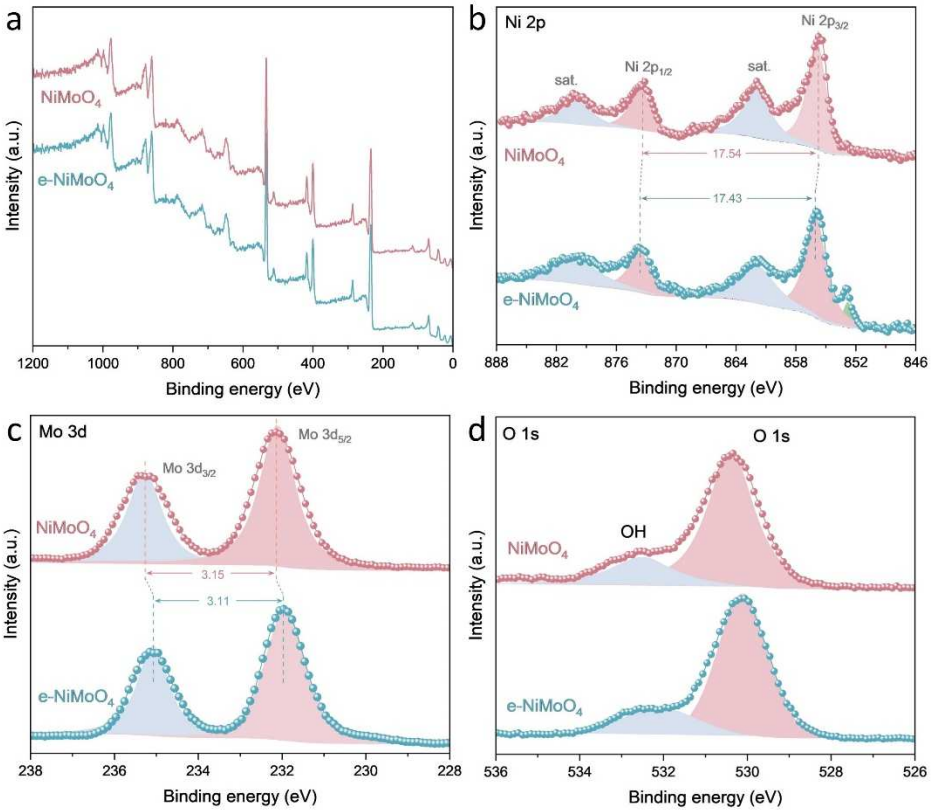

Supplementary Fig. 6 a, Survey spectra of $NiMoO_4$ and e-$NiMoO_4$, **b,** Corresponding high-resolution Ni 2p spectra. **c,** Corresponding high-resolution Mo 3d spectra. **d,** Corresponding high-resolution O 1s spectra.

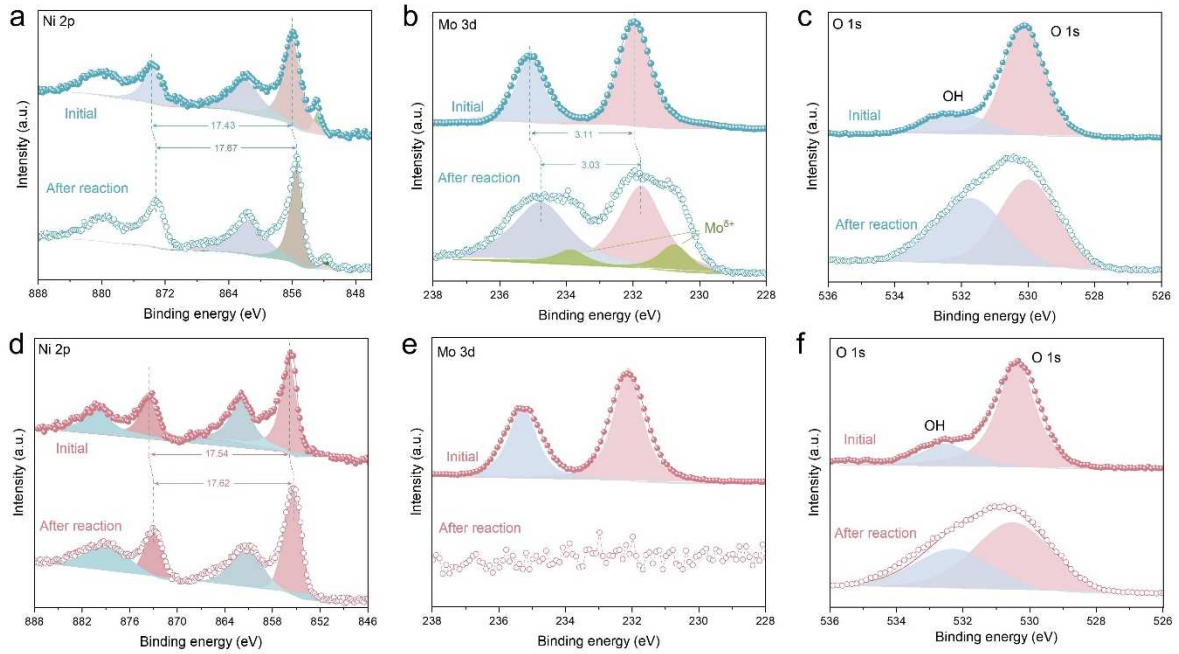

Supplementary Fig. 23 High-resolution XPS spectra of e-$NiMoO_4$ before and after stability testing. **a,** Ni2p. **b,** Mo 3d. **c,** O1s. High-resolution XPS spectra of $NiMoO_4$ before and after

stability testing. **d,** Ni2p. **e,** Mo 3d. **f,** O1s.

i) The slight shift in the XPS O 1s peak is observed in both samples. How is this related to alkaline HER for $NiMoO_4$ and e-$NiMoO_4$?

Our response: Due to the interfacial coupling between $Ni(OH)_2$ and $NiMoO_4$, the electron density at the oxygen sites increases, leading to a negative shift in the O 1s peak of e-$NiMoO_4$ from 531.5 eV to 531.2 eV. After the reaction, the oxidation states of both nickel and molybdenum exhibit a downward shift. For $NiMoO_4$, in addition to the shift of the main oxygen peak, a significant increase in OH content is observed upon activation. In the case of e-$NiMoO_4$, the shift in the O 1s peak is attributed to surface hydroxyl passivation.

"After the electrochemical synthesis and the introduction of $Ni(OH)_2$, the oxidation state of Ni nearly remains unchanged, while that of Mo shifts significantly toward a lower valence state[3]. This observation aligns with the growth mechanism, which involves the balance between surface Mo leaching and the epitaxial growth of $Ni(OH)_2$. Furthermore, the interfacial coupling between $Ni(OH)_2$ and $NiMoO_4$ increases the electron density at the oxygen sites, resulting in a negative shift of the O 1s peak from 531.5 eV to 531.2 eV."***(Page 7 in revised supplementary materials)***

"After the reaction, the oxidation states of both nickel and molybdenum exhibit a downward shift. For $NiMoO_4$, in addition to the shift of the main oxygen peak, a significant increase in OH content is observed upon activation. In the case of e-$NiMoO_4$, the shift in the O 1s peak is attributed to surface hydroxyl passivation."***(Pages 25 in revised supplementary materials)***

ii) In $NiMoO_4$, the Mo XPS peak almost disappears, likely due to Mo dissolution (as described in the manuscript). In contrast, e-$NiMoO_4$ shows a negative shift in both Ni and Mo XPS peaks, along with an increased oxidation state for Mo. This should be explained. As shown in Fig. 3j, there is some question about the claim that Mo in e-$NiMoO_4$ does not participate in any reaction.

Our response: The original figure labeled $Mo^{\delta+}$ with δ+ assigned as 5+, indicating a reduction in oxidation state compared to the pre-reaction condition. To address potential misunderstandings caused by unclear Mo labeling, we have corrected the figure annotations. Additionally, regarding the Mo species in Fig. 3j, a portion of Mo in $NiMoO_4$ spontaneously dissolves in an alkaline medium in the form of molybdate, following the reaction: $NiMoO_4$ (s)

+ $2OH^- \rightarrow Ni(OH)_2$ (s) + MoO_4^{2-} (aq). The corresponding ICP results confirm that after immersing a 1.5×1 cm $NiMoO_4$ sample in 20 mL of 1.0 M KOH with stirring for 10 hours, the Mo concentration in the solution was 14.0 ppm (Supplementary **Table 2**). Since the dissolved Mo does not participate as an active site in the reaction, it cannot contribute to catalytic activity. Meanwhile, the surface of e-$NiMoO_4$ forms a nickel hydroxide passivation layer. Under reaction conditions, ICP analysis determined the Mo concentration to be 0.85 ppm which is lower than that of $NiMoO_4$ (7.08 ppm). Above results confirmed that the active sites in the reaction are exclusively associated with Ni sites.

Supplementary Table 2. The ICP analysis of metal dissolution behavior under both natural and operational conditions.

Testing Conditions	Electrode Soaking (10 h)		HER Reaction (10 h)	
Materials	$NiMoO_4$	e-$NiMoO_4$	$NiMoO_4$	e-$NiMoO_4$
Dissolved Ni (ppm)	0.31	0.11	0.12	0.09
Dissolved Mo (ppm)	14.0	1.89	7.08	0.85

"A portion of Mo in $NiMoO_4$ spontaneously dissolves in an alkaline medium in the form of molybdate. The corresponding ICP results confirm that after immersing a 1.5×1 cm $NiMoO_4$ sample in 20 mL of 1.0 M KOH with stirring for 10 hours, the Mo concentration in the solution was 14.0 ppm."***(Page 23 in revised supplementary materials)***

iii) In the Ni 2p XPS region of e-$NiMoO_4$, a Nix peak (around 857 eV) is observed, which weakens after the HER process. This XPS peak is absent in the $NiMoO_4$. Please provide further explanation regarding this.

Our response: The initial misunderstanding regarding the Ni_x peak (around 857 eV) was caused by an issue with the original figure's color scheme. To clarify this, we have redrawn the spectrum. Additionally, to eliminate potential experimental errors, we conducted new measurements on both $NiMoO_4$ and e-$NiMoO_4$ (**Fig. R2**). The results confirm that the surface structure and peak shift trends remain consistent with the data presented in the original manuscript.

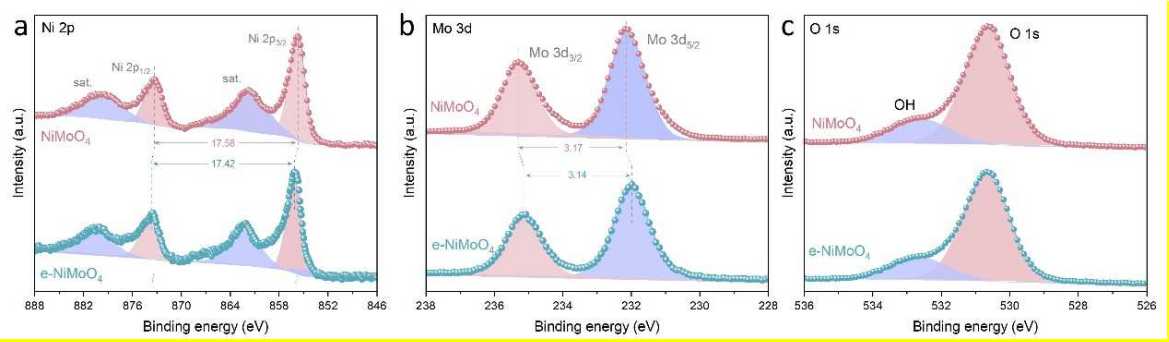

Fig. R2. High-resolution Ni 2p spectra of $NiMoO_4$ and e-$NiMoO_4$. **a,** Corresponding high-resolution Ni 2p spectra. **b,** Corresponding high-resolution Mo 3d spectra. **c,** Corresponding high-resolution O 1s spectra.

Q6: *During electrochemical analysis, is there any activation observed during LSV cycles or CV cycles? Surface reconstruction could occur due to redox reactions under cathodic potential simultaneously with HER.*

Our response: We greatly appreciate your insightful comments. To further investigate the potential activation effects and surface reconstruction during HER, we conducted additional electrochemical activation tests. During the first 10 CV cycles, a slight increase in current density was observed, which can be attributed to improved electrode wettability (Supplementary **Fig. 20**). After 100 CV cycles, no further activation was detected, indicating that the surface structure and composition remained stable following the initial wetting process. These results suggest that under cathodic potential, e-$NiMoO_4$ primarily facilitates the HER process without significant surface reconstruction. The newly supplemented data are summarized below and have been added to the revised manuscript:

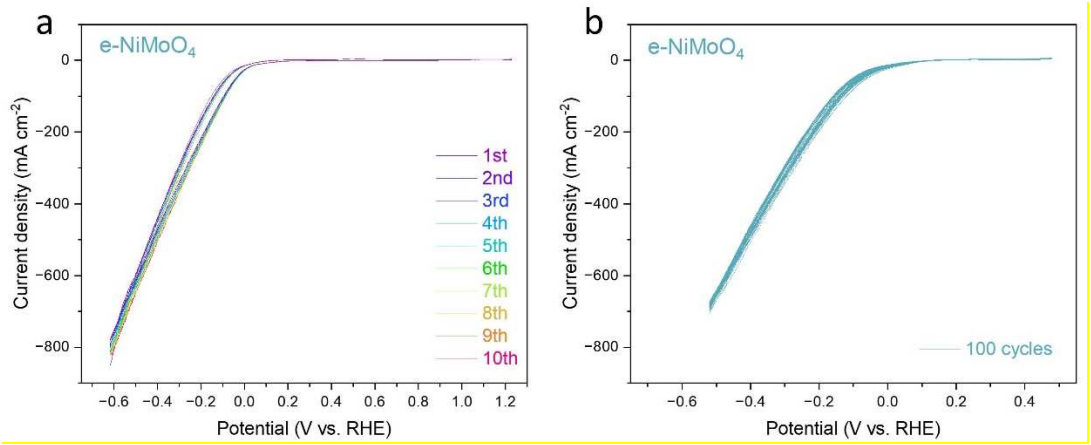

Supplementary Fig. 20 a, Cyclic voltammetry curves of the first ten cycles. **b,** Cyclic

voltammetry curves for 100 cycles.

"Cyclic voltammetry (CV) cycling tests indicate a slight increase in current density after the first 10 cycles, which can be attributed to improved electrode wettability[6]. After 100 cycles, the material maintains stable activity without noticeable redox peaks, ruling out significant redeposition of dissolved species."*(**Page 23 in revised supplementary materials**)*

Supplementary Reference:

6. Liang Y., Han Y., Li J.-s., Wang J., Liu D., Fan Q. Wettability control in electrocatalyst: A mini review. *J. Energy Chem.* **70**, 643-655 (2022).

Q7: *The epitaxial hydroxide layer on the surface may have affected the ECSA. It would be beneficial to compare the ECSA of the e-$NiMoO_4$-1 or $NiMoO_4$-a, where the epitaxial hydroxide layer is minimally formed, with that of the optimized e-$NiMoO_4$ to demonstrate this effect.*

Our response: We sincerely appreciate your suggestions regarding the role of the epitaxial hydroxide layer in modulating the electrochemical surface area (ECSA). To clarify this effect, we synthesized control samples with varying amounts of surface hydroxide layers by adjusting the reconstruction time. SEM images revealed that as the reconstruction time increased (from 1 min to 12 min), the surface roughness significantly increased, indicating that the epitaxial hydroxide layer effectively enhances the surface area (Supplementary **Fig. 11**). Electrochemical surface area calculations, based on CV-derived double-layer capacitance (C_{dl}), further confirmed this effect. With prolonged reconstruction time, the ECSA progressively increased from 27.5 mF cm^{-2} to 98.3 mF cm^{-2}, demonstrating a direct correlation between the roughness induced by the epitaxial $Ni(OH)_2$ layer and ECSA enhancement (Supplementary **Fig. 17**). Interestingly, the sample with the largest active surface area did not exhibit the highest HER activity, suggesting that in the reaction system, HER activity is optimized through the synergistic modulation of the $Ni(OH)_2$-$NiMoO_4$ interfacial structure and ECSA (**Fig. R3**). The newly supplemented data are summarized below and have been added to the revised manuscript:

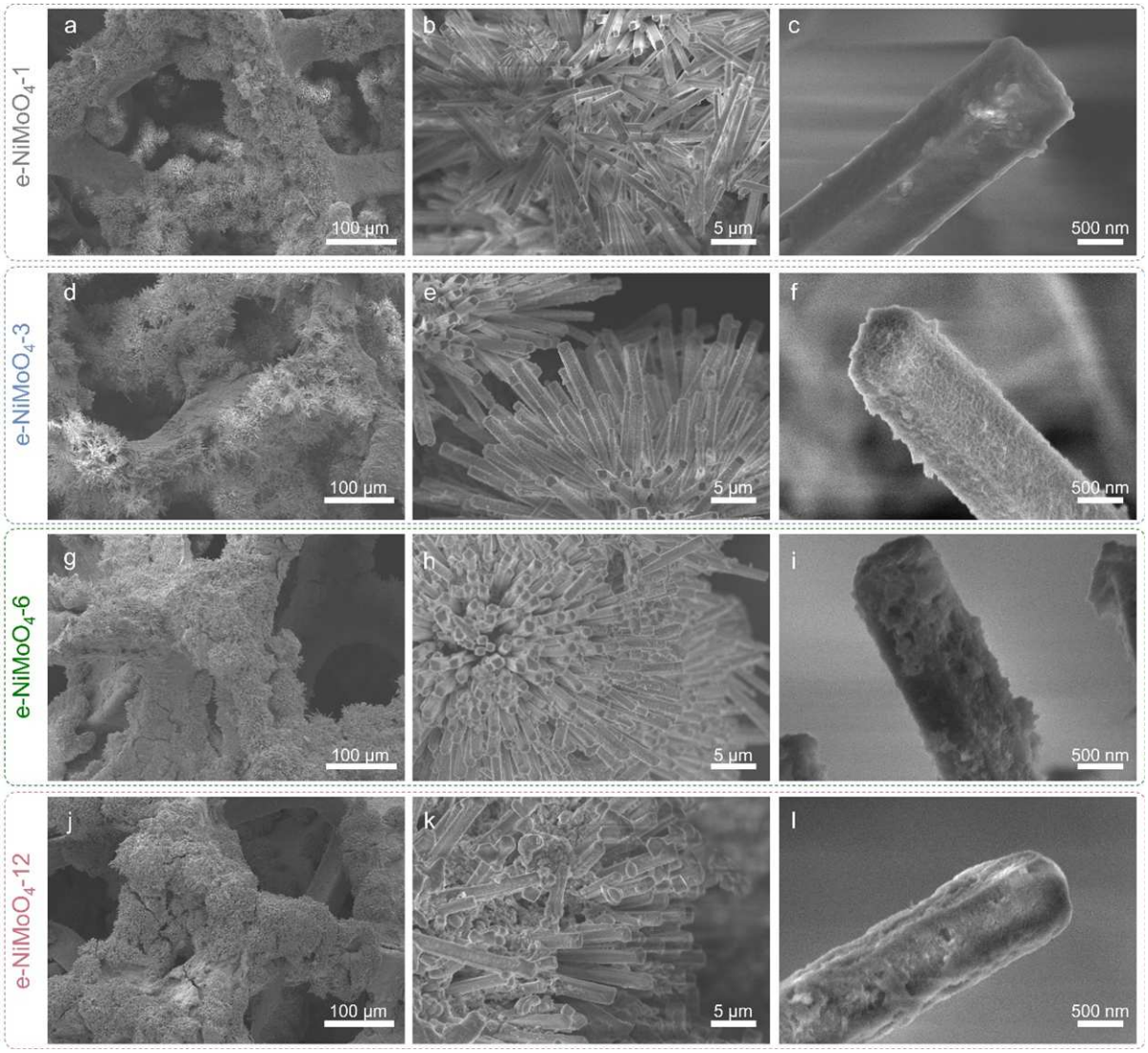

Supplementary Fig. 11 a, b, c, SEM images of e-$NiMoO_4$-1 (1min) at different magnifications. **d, e, f,** SEM images of e-$NiMoO_4$-3 (3min) at different magnification. **g, h, i,** SEM images of e-$NiMoO_4$-6 (6min) at different magnification. **j, k, l,** SEM images of e-$NiMoO_4$-1 (12min) at different magnification.

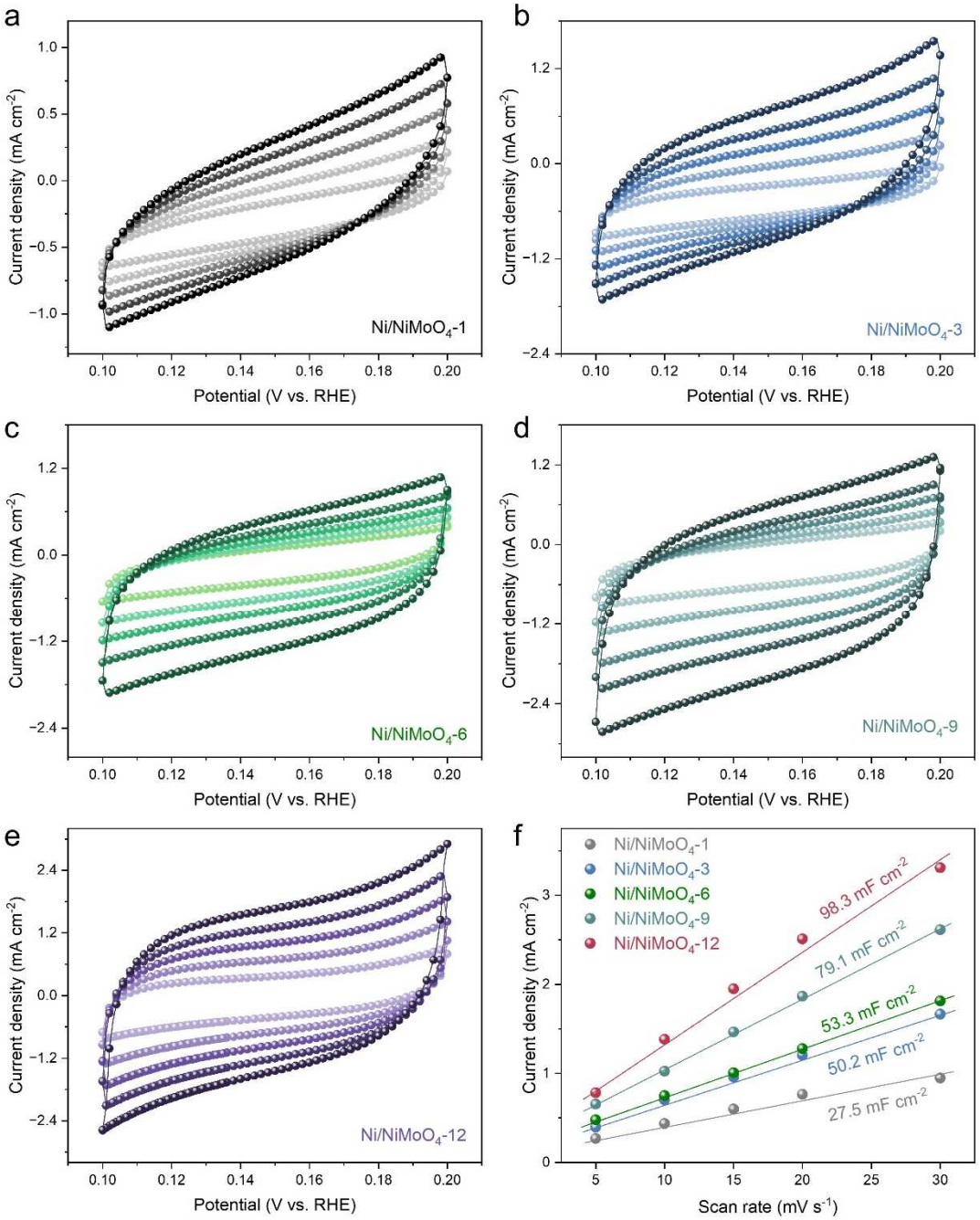

Supplementary Fig. 17 Multiple-measured CV curves of e-$NiMoO_4$ with different reconstruction time. **a,** e-$NiMoO_4$-1. **b,** e-$NiMoO_4$-3. **c,** e-$NiMoO_4$-6. **d,** e-$NiMoO_4$-9. **e,** e-$NiMoO_4$-12. **f,** Corresponding C_{dl} of above five samples.

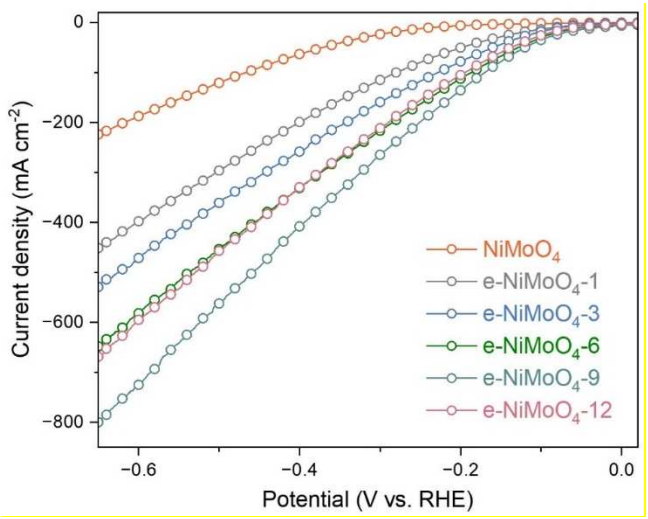

Figure R3. Polarization curves of $NiMoO_4$ and e-$NiMoO_4$ with different reconstruction time (e-$NiMoO_4$-1, 1 min; e-$NiMoO_4$-3, 3 min; e-$NiMoO_4$-6, 6 min; e-$NiMoO_4$-9, 9 min; e-$NiMoO_4$-12, 12 min).

"With increasing reconstruction time (from 1 min to 12 min), the surface roughness significantly increases, indicating that the epitaxial hydroxide layer effectively enhances the surface area[5]. The electrochemical surface area (ECSA) gradually increases from 27.5 mF cm^{-2} to 98.3 mF cm^{-2}, demonstrating a direct correlation between the roughness induced by the epitaxial $Ni(OH)_2$ layer and the enhancement of ECSA. The sample with the largest active surface area did not exhibit the highest HER activity, suggesting that in the reaction system, HER activity is optimized through the synergistic modulation of the $Ni(OH)_2$-$NiMoO_4$ interfacial structure and ECSA."***(Pages 19~20 in revised supplementary materials)***

Supplementary Reference:

5. Davis E. M., Bergmann A., Kuhlenbeck H., Roldan Cuenya B. Facet dependence of the oxygen evolution reaction on Co_3O_4, $CoFe_2O_4$, and Fe_3O_4 epitaxial film electrocatalysts. *J. Am. Chem. Soc.* **146**, 13770-13782 (2024).

Q8: *I recommend performing ICP analysis of the electrolyte to provide evidence of Mo dissolution for e-$NiMoO_4$ and $NiMoO_4$.*

Our response: Thanks for your valuable suggestions. To assess the dissolution behavior of Mo, we performed ICP analysis on the electrolyte with and without applied potential for both e-$NiMoO_4$ and $NiMoO_4$. The results clearly indicate a certain degree of Mo dissolution, with

specific quantitative data presented in Supplementary **Table 2**. For $NiMoO_4$, Mo dissolves primarily in the form of MoO_4^{2-} (molybdate), while the deposition of $Ni(OH)_2$ leads to partial structural degradation, accelerating Mo release. This process represents a continuous chemical dissolution. In contrast, the surface dendritic layer of reconstructed e-$NiMoO_4$ significantly suppresses Mo dissolution.

Supplementary Table 2. The ICP analysis of metal dissolution behavior under both natural and operational conditions.

Testing Conditions	Electrode Soaking (10 h)		HER Reaction (10 h)	
Materials	$NiMoO_4$	e-$NiMoO_4$	$NiMoO_4$	e-$NiMoO_4$
Dissolved Ni (ppm)	0.31	0.11	0.12	0.09
Dissolved Mo (ppm)	14.0	1.89	7.08	0.85

"A portion of Mo in $NiMoO_4$ spontaneously dissolves in an alkaline medium in the form of molybdate. The corresponding ICP results confirm that after immersing a 1.5×1 cm $NiMoO_4$ sample in 20 mL of 1.0 M KOH with stirring for 10 hours, the Mo concentration in the solution was 14.0 ppm."***(Page 23 in revised supplementary materials)***

Reviewer #2 (Comments to the Author): ==========

Alkaline electrolyzers are currently the most widely adopted technology for large-scale industrial hydrogen production. In this study, Chang and his colleagues investigated the challenges related to the Volmer step of the alkaline water dissociation reaction, as well as the slow kinetics caused by the subsequent desorption of OH species. Unlike the conventional focus on optimizing the chemical and electronic structures of catalysts, their research centered on the often-overlooked structure of the EDL within the electrolyte. By synchronizing the regulation and optimization of the catalyst-electrolyte interface active sites and the EDL structure, their study gained valuable insights. They demonstrated that the dynamically constructed epitaxial hydroxide layer serves as a protective barrier against molybdenum leaching, significantly enhancing material stability. The dendritic epitaxial layer also intensified the local electric field, optimizing the electrochemical environment at the catalyst-electrolyte interface and thereby accelerating reaction kinetics. Most notably, the optimized material exhibited excellent activity and stability when directly evaluated within an industrial assessment system. This comprehensive study unveiled intriguing experimental phenomena and was thoroughly supported by data analysis, elucidating the complexities of the reaction mechanism and its potential applications in industrial systems.*

After careful review, I would like to recommend its acceptance in Nature Communications after revision. The following suggestions are provided for the authors:

Our response: We sincerely appreciate your recognition and encouraging comments on manuscript. We carefully considered all comments and provided a point-by-point response as outlined below:

Specific comments:

Q1: *The authors primarily focused on the changes in the coordination structure of nickel during material structural analysis. To strengthen this analysis, it is recommended to include XAFS analysis of Mo in both $NiMoO_4$ and e-$NiMoO_4$ structures, as well as their post-reaction states. This will help to emphasize the structural advantages of e-$NiMoO_4$.*

Our response: We appreciate your comments and have incorporated additional XAFS analysis of Mo. In electrochemically synthesized e-$NiMoO_4$, the Mo coordination environment remains similar to that of $NiMoO_4$, with a slight increase in Mo-O bond length (Supplementary **Fig. 8**). These results indicate that Mo dissolution leads to minor structural loosening while preserving

the overall integrity of the Mo-containing framework, highlighting the stability and structural flexibility of the epitaxially grown $Ni(OH)_2$ dendritic layer.

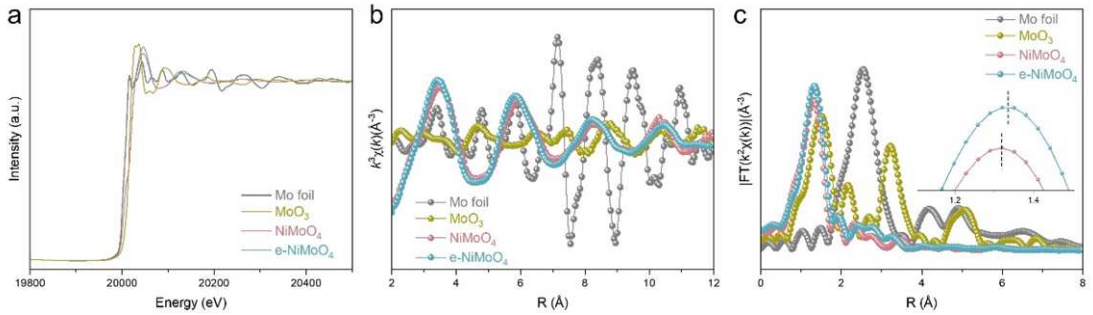

Supplementary Fig. 8 a, Mo K-edge XANES spectra of $NiMoO_4$, e-$NiMoO_4$, Mo foil and MoO_3. **b,** The corresponding k space for Mo K-edge. **c,** The corresponding Fourier transformed magnitudes of Mo K-edge EXAFS spectra.

"Meanwhile, the bonding coordination environment of Mo has been further analyzed (Supplementary Fig. 8). The Mo coordination environment of e-$NiMoO_4$ is similar to that of $NiMoO_4$, with a slight increase in the Mo-O bond length. These findings indicate that Mo dissolution causes minor structural loosening while preserving the overall integrity of the Mo-containing framework, highlighting the stability and structural flexibility of the epitaxially grown $Ni(OH)_2$ dendritic layer."***(Page 6 in revised manuscript)***

Q2: *The synthesis time and voltage in electrochemical processes are two critical factors. It is suggested to conduct electrochemical analysis on samples with varying reconstruction times. Additionally, incorporating a synthesis schematic would provide a clearer understanding of the synthesis mechanism.*

Our response: We appreciate your insightful comments. We optimized the materials preparation by varying synthesis time. SEM images reveal that as the synthesis time increases (from 1 min to 12 min), surface roughness significantly increases, indicating that the epitaxial hydroxide layer effectively enhances the surface area (Supplementary **Fig. 11**). Correspondingly, the electrochemical surface area increases from 27.5 mF cm^{-2} to 98.3 mF cm^{-2}, demonstrating a direct correlation between surface roughness induced by the epitaxial $Ni(OH)_2$ layer and ECSA enhancement (Supplementary **Fig. 17**). However, the sample with the largest active surface area does not exhibit the highest HER activity, suggesting that optimal HER performance results from a balanced interplay between the $Ni(OH)_2$-$NiMoO_4$ interface

structure and ECSA.

Additionally, we analyzed the influence of electrochemical synthesis voltage on material formation (Supplementary **Fig. 10** and **15**). At low synthesis voltages, the material surface remains smooth with no significant structural changes. In contrast, excessively high voltages lead to severe surface etching, extensive dissolution of the nanorod substrate, and substantial $Ni(OH)_2$ deposition on the remaining nanorods. The reconstruction time also directly affects the growth rate of the $Ni(OH)_2$ layer. The entire process follows a balance between nanorod etching and $Ni(OH)_2$ growth.

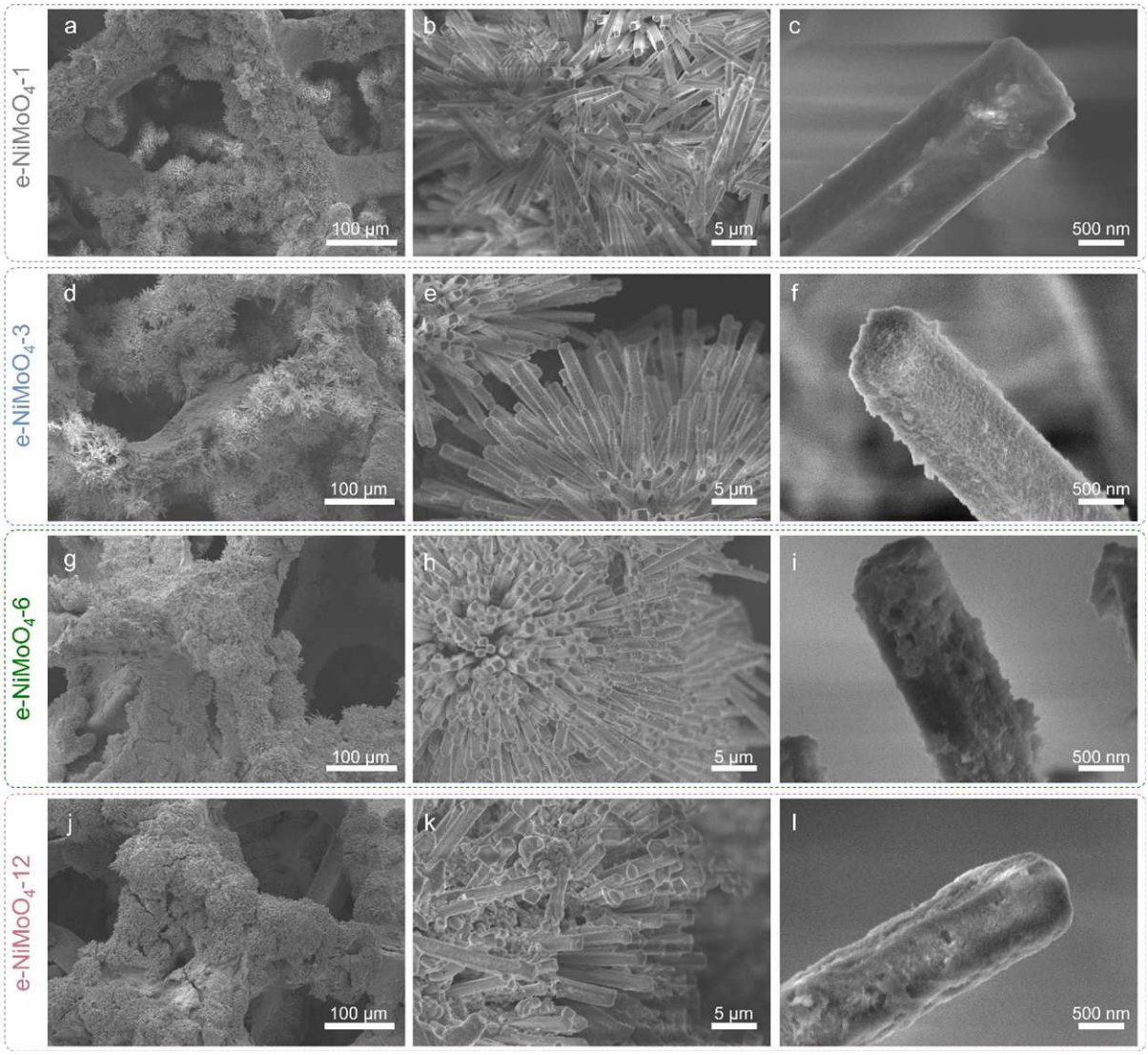

Supplementary Fig. 11 a, b, c, SEM images of e-$NiMoO_4$-1 (1min) at different magnifications. **d, e, f,** SEM images of e-$NiMoO_4$-3 (3min) at different magnification. **g, h, i,** SEM images of e-$NiMoO_4$-6 (6min) at different magnification. **j, k, l,** SEM images of e-$NiMoO_4$-1 (12min) at different magnification.

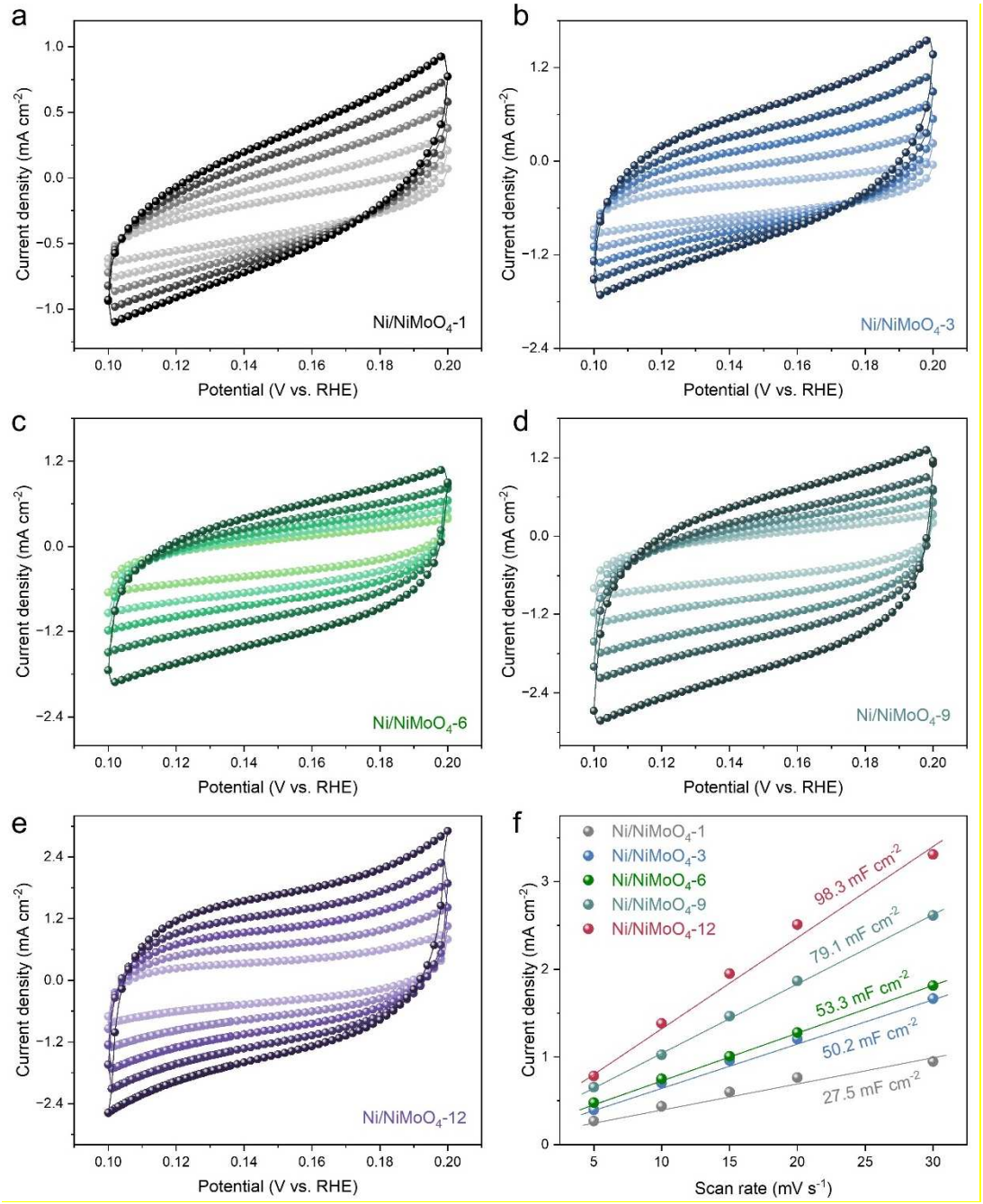

Supplementary Fig. 17 Multiple-measured CV curves of e-$NiMoO_4$ with different reconstruction time. **a,** e-$NiMoO_4$-1. **b,** e-$NiMoO_4$-3. **c,** e-$NiMoO_4$-6. **d,** e-$NiMoO_4$-9. **e,** e-$NiMoO_4$-12. **f,** Corresponding C_{dl} of above five samples.

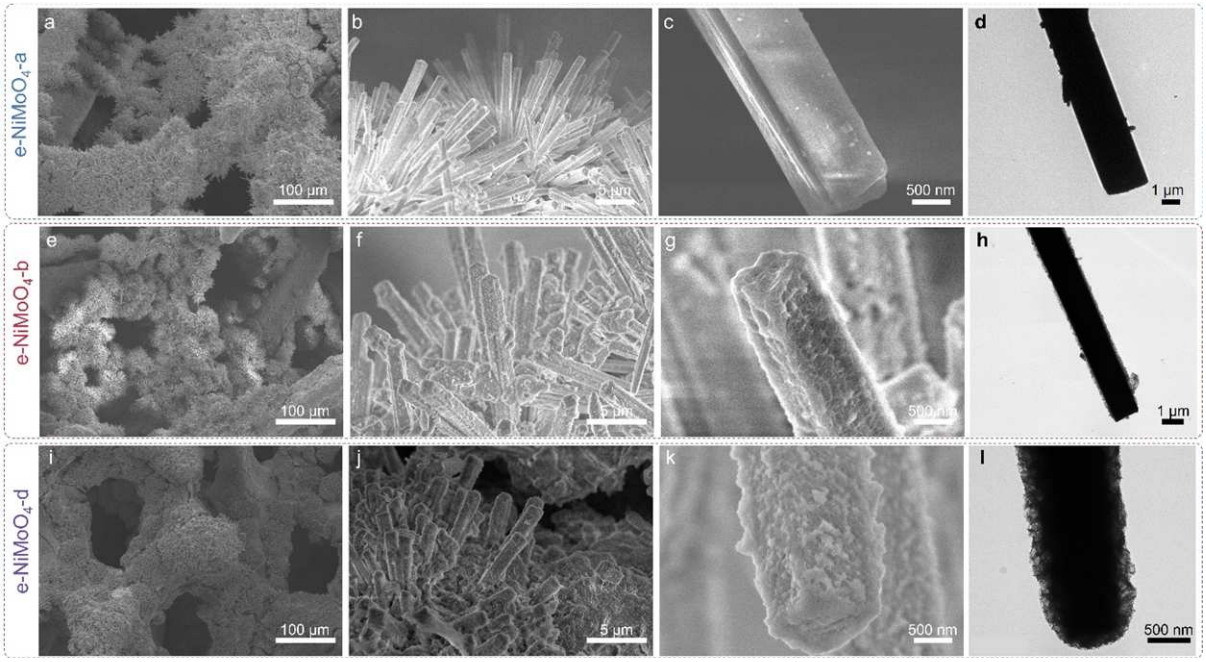

Supplementary Fig. 10 a, b, c, SEM images of e-NiMoO₄-a (-0.085 V) at different magnification. **d,** TEM image of e-NiMoO₄-a (-0.085 V). **e, f, g,** SEM images of e-NiMoO₄-a (-0.285 V) at different magnification. **h,** TEM image of e-NiMoO₄-a (-0.285 V). **i, j, k,** SEM images of e-NiMoO₄-a (-0.685 V) at different magnification. **l,** TEM image of e-NiMoO₄-a (-0.685 V).

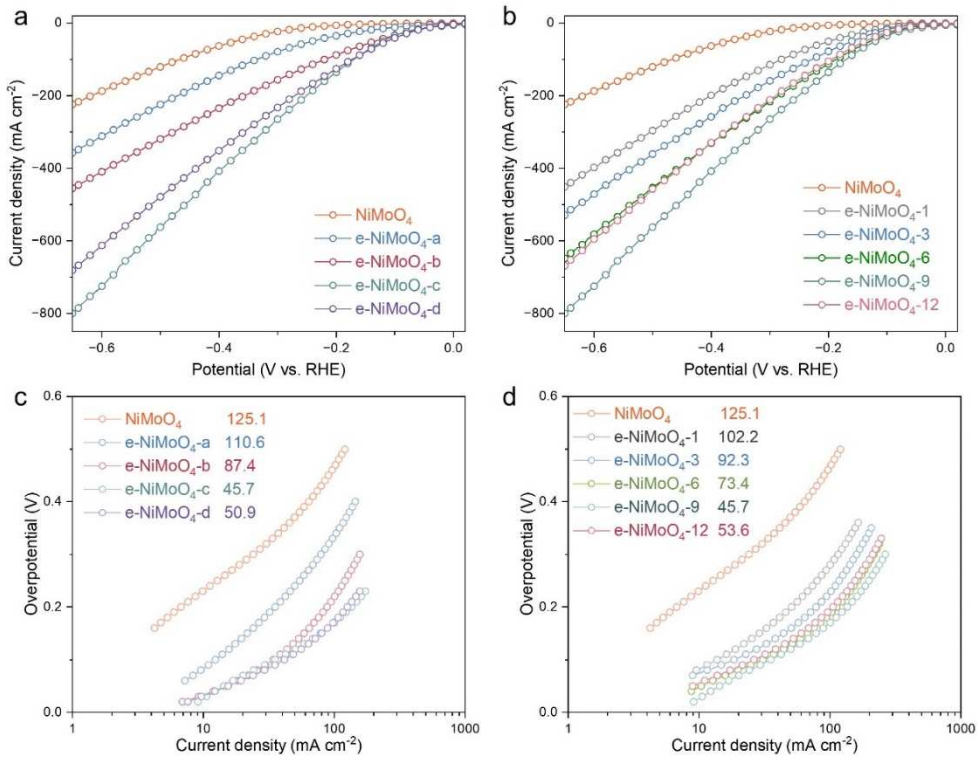

Supplementary Fig. 15 a, Polarization curves of NiMoO₄ and e-NiMoO₄ with different

reconstruction potential (e-$NiMoO_4$-a, -0.085 V; e-$NiMoO_4$-a, -0.285 V; e-$NiMoO_4$-a, -0.485 V; e-$NiMoO_4$-a, -0.685 V;), **c,** Corresponding tafel analysis of **a**. **b,** Polarization curves of $NiMoO_4$ and e-$NiMoO_4$ with different reconstruction time (e-$NiMoO_4$-1, 1 min; e-$NiMoO_4$-3, 3 min; e-$NiMoO_4$-6, 6 min; e-$NiMoO_4$-9, 9 min; e-$NiMoO_4$-12, 12 min), **d,** Corresponding tafel analysis of **c**.

"The electrochemical synthesis was optimized by adjusting the cathodic potential, synthesis duration, and electrochemical parameters for different electrode sizes to obtain the optimal e-$NiMoO_4$ with varying sizes (Supplementary Fig. 9-14)." ***(Page 6 in revised manuscript)***

"With increasing reconstruction time (from 1 min to 12 min), the surface roughness significantly increases, indicating that the epitaxial hydroxide layer effectively enhances the surface area[5]. The electrochemical surface area (ECSA) gradually increases from 27.5 mF cm^{-2} to 98.3 mF cm^{-2}, demonstrating a direct correlation between the roughness induced by the epitaxial $Ni(OH)_2$ layer and the enhancement of ECSA. The sample with the largest active surface area did not exhibit the highest HER activity, suggesting that in the reaction system, HER activity is optimized through the synergistic modulation of the $Ni(OH)_2$-$NiMoO_4$ interfacial structure and ECSA." ***(Pages 19~20 in revised supplementary materials)***

Supplementary Reference:

5. Davis E. M., Bergmann A., Kuhlenbeck H., Roldan Cuenya B. Facet dependence of the oxygen evolution reaction on Co_3O_4, $CoFe_2O_4$, and Fe_3O_4 epitaxial film electrocatalysts. *J. Am. Chem. Soc.* **146**, 13770-13782 (2024).

Q3: *Based on findings from in-situ XAFS tests, it was observed that the control sample NiMoO4 underwent significant structural collapse and transformation into hydroxides after prolonged cycling, whereas e-$NiMoO_4$ did not exhibit these changes. Including relevant characterization data would offer a more direct visualization of the morphological changes in the two samples post-cycling.*

Our response: We greatly appreciate your constructive comment. To directly compare the morphological differences between $NiMoO_4$ and e-$NiMoO_4$ after cycling, we conducted post-cycling TEM analysis (Supplementary **Fig. 21**). The $NiMoO_4$ sample exhibited severe structural collapse and agglomeration, accompanied by a transformation into a loose hydroxide

layer, consistent with the in situ XAFS observations. In contrast, while e-$NiMoO_4$ showed slight collapse and agglomeration, it largely retained its original morphology and the epitaxial $Ni(OH)_2/NiMoO_4$ interface, without significant phase transitions or structural degradation. These findings directly confirm the structural stability of e-$NiMoO_4$ under prolonged HER operation, which is attributed to the protective epitaxial hydroxide layer mitigating hydroxide phase reconstruction.

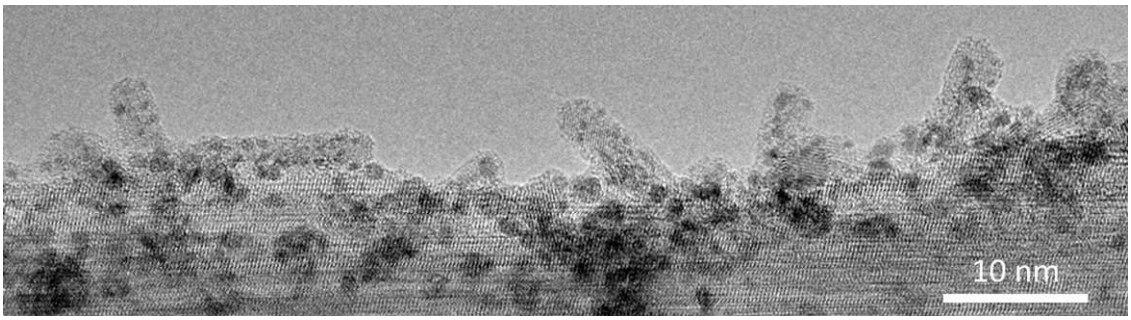

Supplementary Fig. 21 TEM image of e-$NiMoO_4$ after reaction.

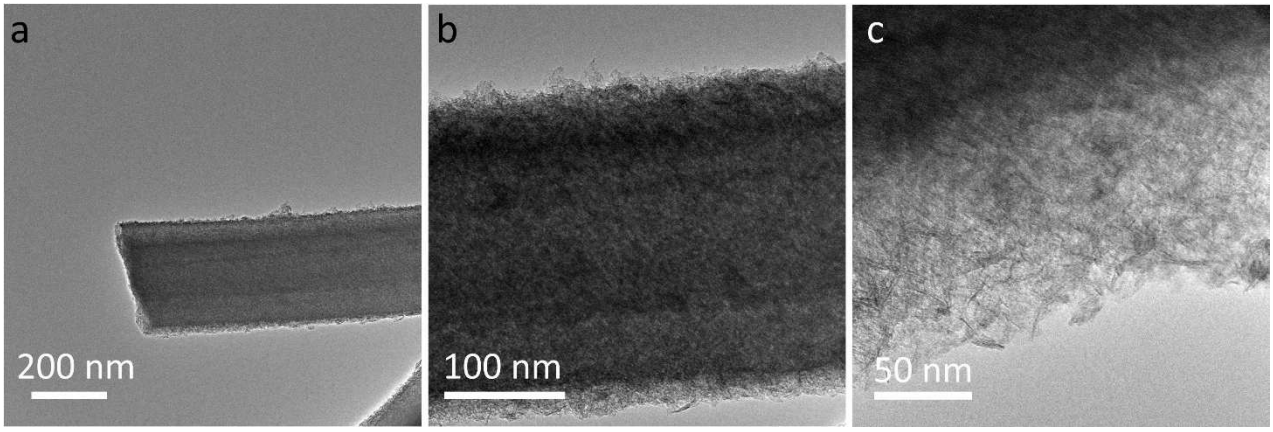

Supplementary Fig. 22 a, b, c, TEM image of e-$NiMoO_4$ after reaction at different magnifications.

"e-$NiMoO_4$ and $NiMoO_4$ were subjected to HER conditions (-0.2 V vs. RHE) in 1.0 M KOH for 10 hours. A thick layer of $Ni(OH)_2$ nanosheets formed on the $NiMoO_4$ surface, whereas the $Ni(OH)_2$ dendritic layer on e-$NiMoO_4$ remained largely intact, with only minor particle aggregation."***(Page 24 in revised supplementary materials)***

Q4: *The electrochemical results presented in this manuscript indicate a clear trend: as the catalytic activity of $NiMoO_4$ samples improves, there is a corresponding decrease in the Tafel slope. This relationship remains consistent even when varying both the reconstruction potential*

and reconstruction time (as shown in Supplementary Fig. 10 and 26). Given that the Tafel slope provides significant insights into the rate-determining step and reaction mechanism in the HER, rather than merely describing catalytic performance, it is essential for the authors to provide a more comprehensive discussion of the underlying mechanistic implications based on the electrochemical data.

Our response: We appreciate your thorough review and valuable comments. The Tafel slope decreased from 125.1 mV/dec for $NiMoO_4$ to 45.7 mV/dec for e-$NiMoO_4$, clearly indicating a transition in the alkaline HER mechanism (**Fig. R5**). For $NiMoO_4$, the high Tafel slope (~120 mV/dec) is consistent with a Volmer–Heyrovsky pathway, where the rate-determining step (RDS) is the dissociation of H_2O (Volmer step: $H_2O + e^- \rightarrow H^* + OH^-$), followed by electrochemical desorption (Heyrovsky step: $H^* + H_2O + e^- \rightarrow H_2 + OH^-$). The sluggish kinetics may be attributed to the poor activation of H_2O and the strong H* adsorption on the $NiMoO_4$ surface. In contrast, e-$NiMoO_4$ exhibits a significantly lower Tafel slope (~40 mV/dec), suggesting a transition to a Volmer-Tafel pathway, where the RDS shifts to the chemical recombination of adsorbed H* (Supplementary **Fig. 15**). This transition is attributed to the epitaxial $Ni(OH)_2/NiMoO_4$ interface, which optimizes H* adsorption energy and facilitates rapid H* coupling. The consistency of this trend across different electrochemical synthesis conditions and reaction pH conditions underscores the critical role of interfacial electronic modulation in redefining the HER pathway, rather than mere surface nanostructural effects (Supplementary **Fig. 45**).

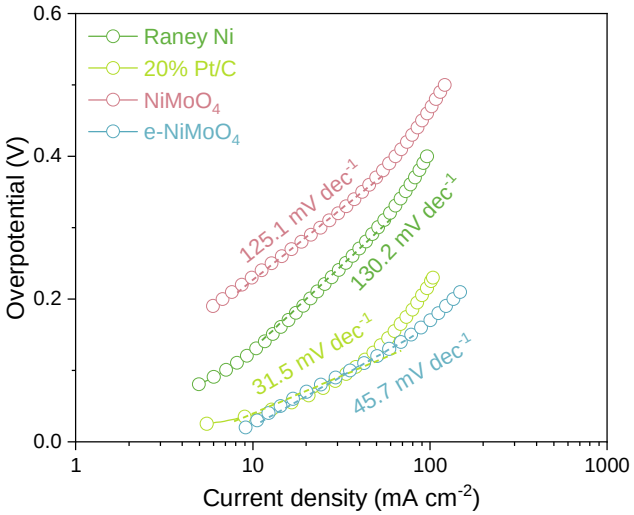

Fig. R5. Tafel analysis of e-$NiMoO_4$ and control samples

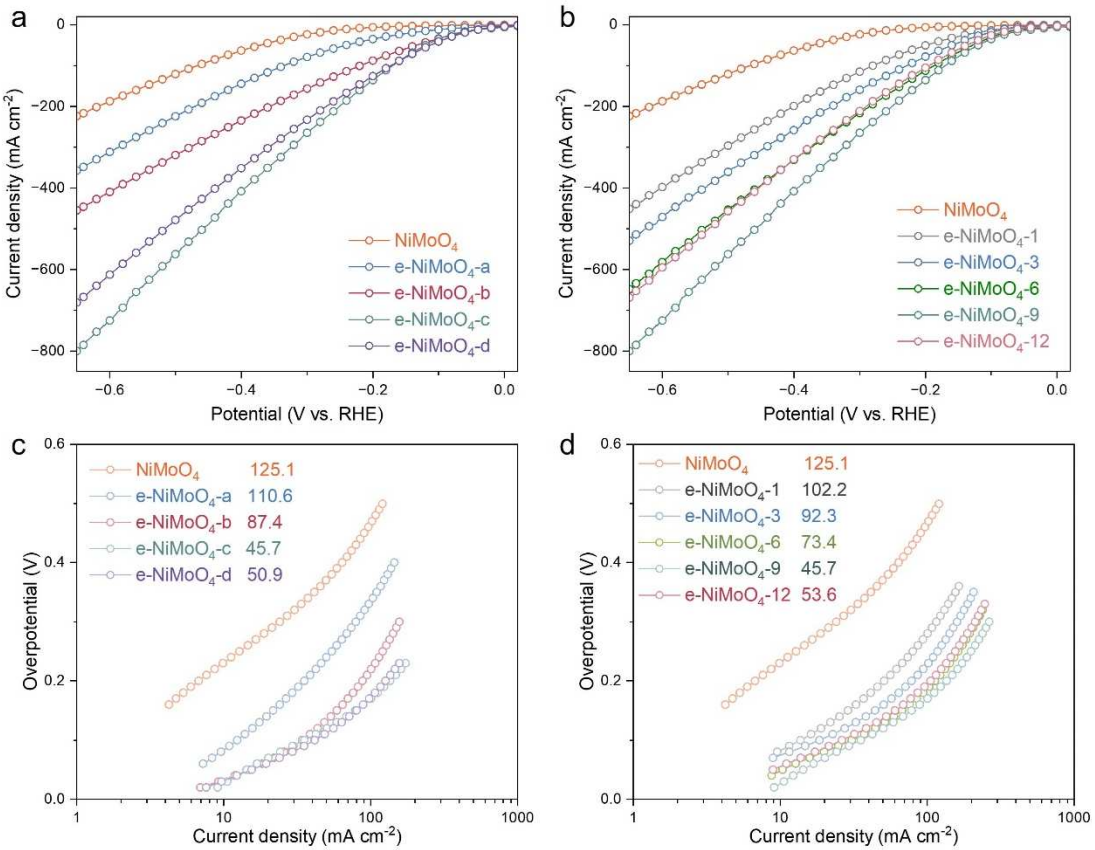

Supplementary Fig. 15 a, Polarization curves of $NiMoO_4$ and e-$NiMoO_4$ with different reconstruction potential (e-$NiMoO_4$-a, -0.085 V; e-$NiMoO_4$-a, -0.285 V; e-$NiMoO_4$-a, -0.485 V; e-$NiMoO_4$-a, -0.685 V;), **c,** Corresponding tafel analysis of **a**. **b,** Polarization curves of $NiMoO_4$ and e-$NiMoO_4$ with different reconstruction time (e-$NiMoO_4$-1, 1 min; e-$NiMoO_4$-3, 3 min; e-$NiMoO_4$-6, 6 min; e-$NiMoO_4$-9, 9 min; e-$NiMoO_4$-12, 12 min), **d,** Corresponding tafel analysis of **c**.

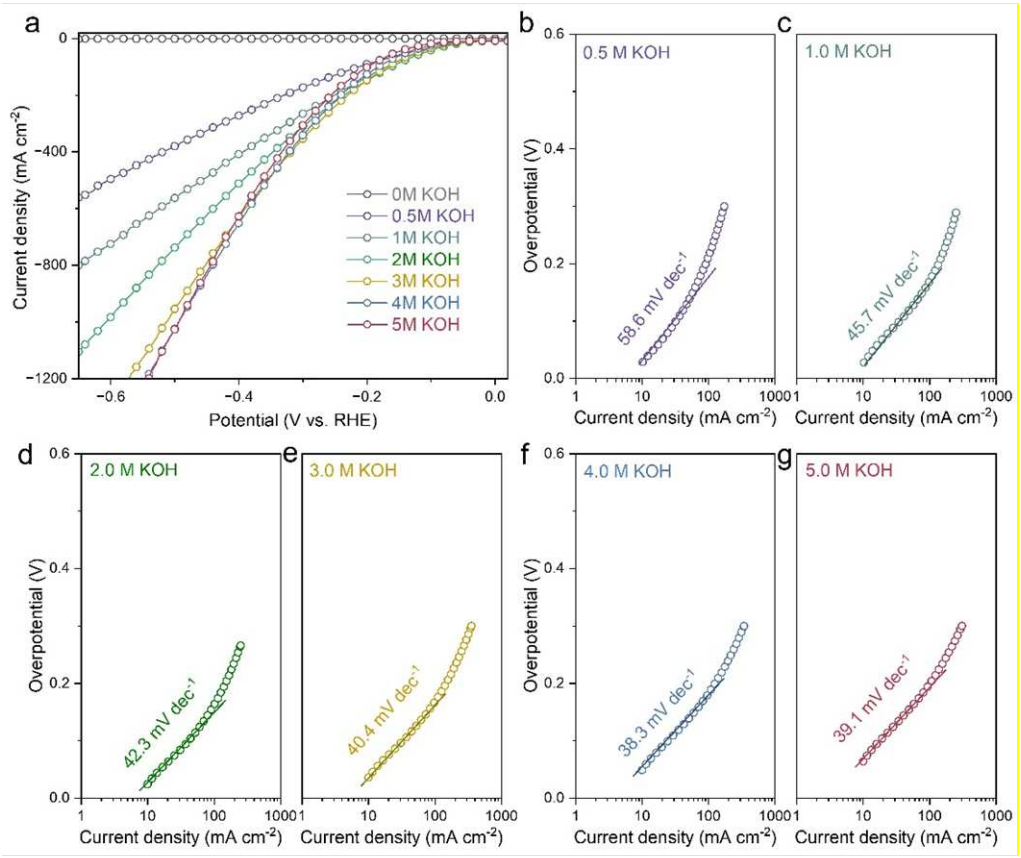

Supplementary Fig. 44 a, Polarization curves of e-NiMoO4 in different concentration KOH solutions. Corresponding tafel analysis of a. **b,** 0.5 M KOH. **c,** 1.0 M KOH. **d,** 2.0 M KOH. **e,** 3.0 M KOH. **f,** 4.0 M KOH. **g,** 5.0 M KOH.

"The variation in Tafel slope indicates a transition in the alkaline HER mechanism. For $NiMoO_4$, the high Tafel slope (~120 mV/dec) aligns with the Volmer–Heyrovsky pathway, where the rate-determining step (RDS) is the dissociation of H_2O (Volmer step: $H_2O + e^- \rightarrow H^* + OH^-$), followed by electrochemical desorption (Heyrovsky step: $H^* + H_2O + e^- \rightarrow H_2 + OH^-$) [33]. The $NiMoO_4$ surface exhibits strong H* adsorption but poor H_2O activation. In contrast, e-$NiMoO_4$ displays a significantly lower Tafel slope (~40 mV/dec), indicating a shift to the Volmer–Tafel pathway, where the RDS transitions to the chemical recombination of adsorbed H*. This transformation is attributed to the epitaxial $Ni(OH)_2/NiMoO_4$ interface, which optimizes H* adsorption energy and facilitates rapid H* coupling."***(Page 7 in revised manuscript)***

Reference:

33. Fu H. Q., *et al.* Hydrogen spillover-bridged volmer/tafel processes enabling ampere-level current density alkaline hydrogen evolution reaction under low overpotential. *J.*

Am. Chem. Soc. **144**, 6028-6039 (2022).

Q5: *Regarding the DFT models, it is crucial to verify whether a k-point optimization was performed. The impact of low-coordination oxygen atoms on the Fermi level in the lower slab should also be considered. Moreover, the authors should investigate how the introduction of K+ influences surface adsorption energy and reaction pathways during modeling.*

Our response: We sincerely appreciate your rigorous comments.

i) k-point convergence: A systematic k-point optimization was performed using the Monkhorst-Pack grid, confirming that a 4 × 4 × 1 k-point mesh achieves energy convergence within 1 meV per atom (Supplementary **Table 6**.). The relative energy differences obtained using different k-point densities fall within an acceptable error range, ensuring the accuracy of the electronic structure calculations.

Supplementary Table 6. *k*-point optimization parameters.

	K point density	System energy (eV)	Atomic average energy (eV)	Relative energy (eV)
$NiMoO_4$	2 × 2 × 1	-1030.8672	-7.5799	
	3 × 3 × 1	-1030.7413	-7.5790	0.0009
	4 × 4 × 1	-1030.8692	-7.5799	0.0000
e-$NiMoO_4$	2 × 2 × 1	-1473.5821	-10.8352	
	3 × 3 × 1	-1473.5073	-10.8346	0.0006
	4 × 4 × 1	-1473.3938	-10.8338	0.0014

ii) Low-coordination oxygen effect: The projected density of states (PDOS) analysis based on the slab model clearly illustrates the presence of low-coordination surface oxygen atoms (Supplementary **Fig. 31**). The PDOS results confirm that these oxygen atoms at the bottom of slab models contribute minimally to the electronic states near the Fermi level, which shows that the constructed slab model is reasonable. We further compared the typical indicator (O*2p* band center and $\Delta_{O2p,Ni3d}$) to evaluate the stability of lattice oxygen species. Both indicators for the two samples are negative and exhibit minimal differences (**Fig. R4**), indicating that oxygen is chemically inert and does not serve as an active site. Specifically, surface oxygen atoms contribute interaction and stabilize the epitaxial interface, thereby preventing lattice distortion during the HER process. The newly supplemented data are summarized below and

have been added to the revised manuscript:

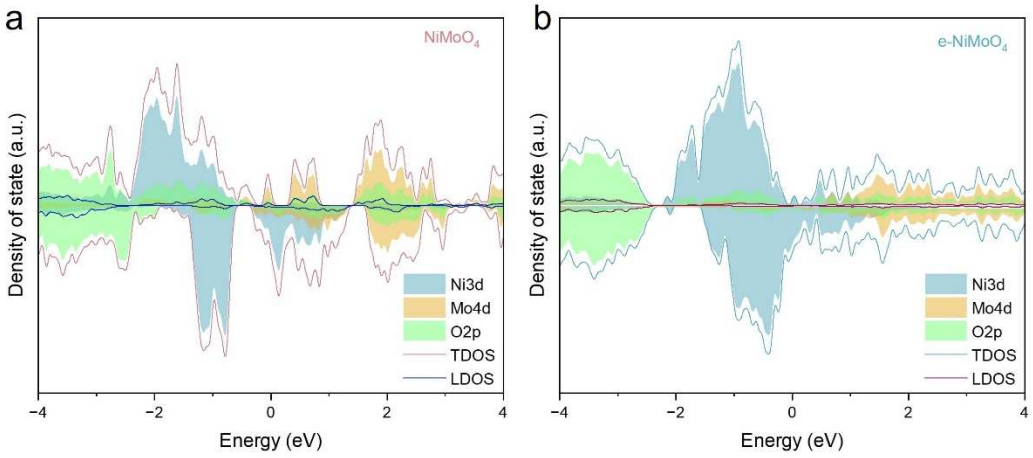

Supplementary Fig. 31 Calculated projected density of states of $NiMoO_4$ (**a**) and e-$NiMoO_4$ (**b**) with total density of states and local density of states.

Supplementary Table 7. *s*,*p*,*d*-center of $NiMoO_4$ and e-$NiMoO_4$.

$NiMoO_4$	Spin-Channel	*s* band center (eV)	*p* band center (eV)	*d* band center (eV)
Mix	Spin-up	-6.311	-3.908	-1.660
	Spin-down	-6.279	-3.772	-0.795
Ni	Spin-up	-2.264	-2.784	-2.438
	Spin-down	-2.329	-2.695	-0.966
Mo	Spin-up	-6.732	-6.876	-0.780
	Spin-down	-6.657	-6.859	-0.605
O	Spin-up	-6.918	-3.400	-
	Spin-down	-6.855	-3.240	-
e-$NiMoO_4$	Spin-Channel	*s* band center (eV)	*p* band center (eV)	*d* band center (eV)
Mix	Spin-up	-7.110	-4.111	-1.346
	Spin-down	-7.106	-4.040	-0.860
Ni	Spin-up	-2.785	-2.535	-1.579
	Spin-down	-2.828	-2.485	-0.862
Mo	Spin-up	-7.699	-7.805	-0.903
	Spin-down	-7.669	-7.770	-0.857
O	Spin-up	-7.941	-3.670	-
	Spin-down	-7.923	-3.591	-

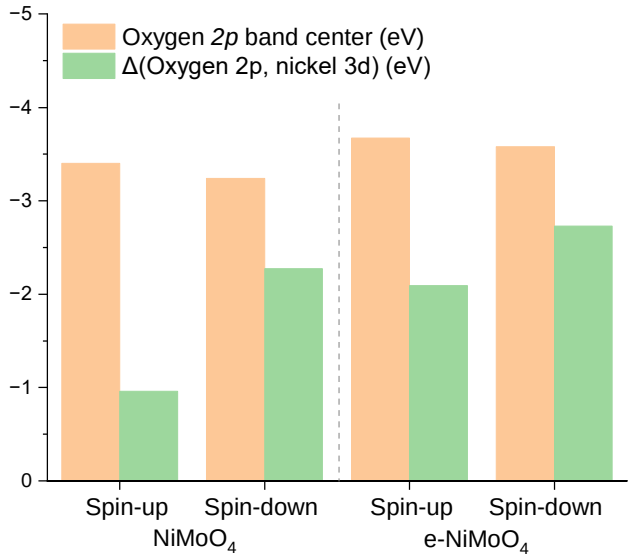

Figure R4. Comparison of O*2p* band center and Δ(O*2p*, Ni*3d*) on $NiMoO_4$ and e-$NiMoO_4$.

"Significant hybridization are observed among the Ni 3*d*, Mo 4*d*, and O 2*p* orbitals, with the centers of the Mo 4d and O 2p orbitals shifting downward relative to the Fermi level (Fig. 4a-b and Supplementary Table 7). Low-coordination surface oxygen exhibit minimal contribution to the electronic states near the Fermi level (Supplementary Fig. S31). Through strong bonding interactions with adjacent Ni and Mo atoms, these oxygen atoms stabilize the epitaxial interface."***(Page 10 in revised manuscript)***

"Projected density of states (PDOS) analysis based on the slab model confirms the presence of low-coordination surface oxygen atoms. The PDOS results confirm that these oxygen atoms at the bottom of slab models contribute minimally to the electronic states near the Fermi level, which shows that the constructed slab model is reasonable. The typical indicator (O*2p* band center and $\Delta_{O2p,Ni3d}$) are negative and exhibit minimal differences, indicating that oxygen is chemically inert and does not serve as an active site. Through strong bonding interactions with neighboring Ni and Mo atoms, these oxygen atoms stabilize the epitaxial interface, thereby preventing lattice distortion during the HER process."***(Page 33 in revised supplementary materials)***

iii) K^+ interaction mechanisms: To elucidate the detailed mechanism by which K^+ optimizes the alkaline HER pathway, we introduced K^+ ions near the active sites (Supplementary **Fig. 38**). On the e-$NiMoO_4$ surface, the dissociation barrier of H_2O is 0.69 eV, primarily due to the sluggish cleavage of the O-H bond. The water activation barrier on K sites on e-$NiMoO_4$ remains excessively high, limiting its catalytic efficiency. In contrast, at the Ni site adjacent to

K^+, the free energy barrier for the conversion of H_2O to OH-H is reduced, thereby facilitating faster OH*-H* decoupling. Overall, the synergistic effect of K^+ is evident in the free energy landscape. While K^+ lowers the Volmer barrier, its primary role lies in rebalancing the H* adsorption–desorption equilibrium, which aligns well with experimental observations. The newly supplemented data are summarized below and have been added to the revised manuscript:

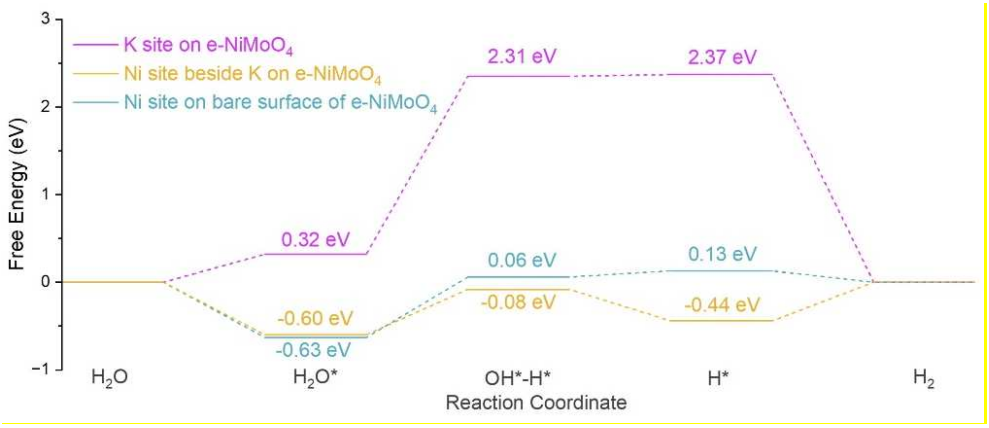

Supplementary Fig. 38. Free energy profile for the alkaline HER process on different sites on e-$NiMoO_4$.

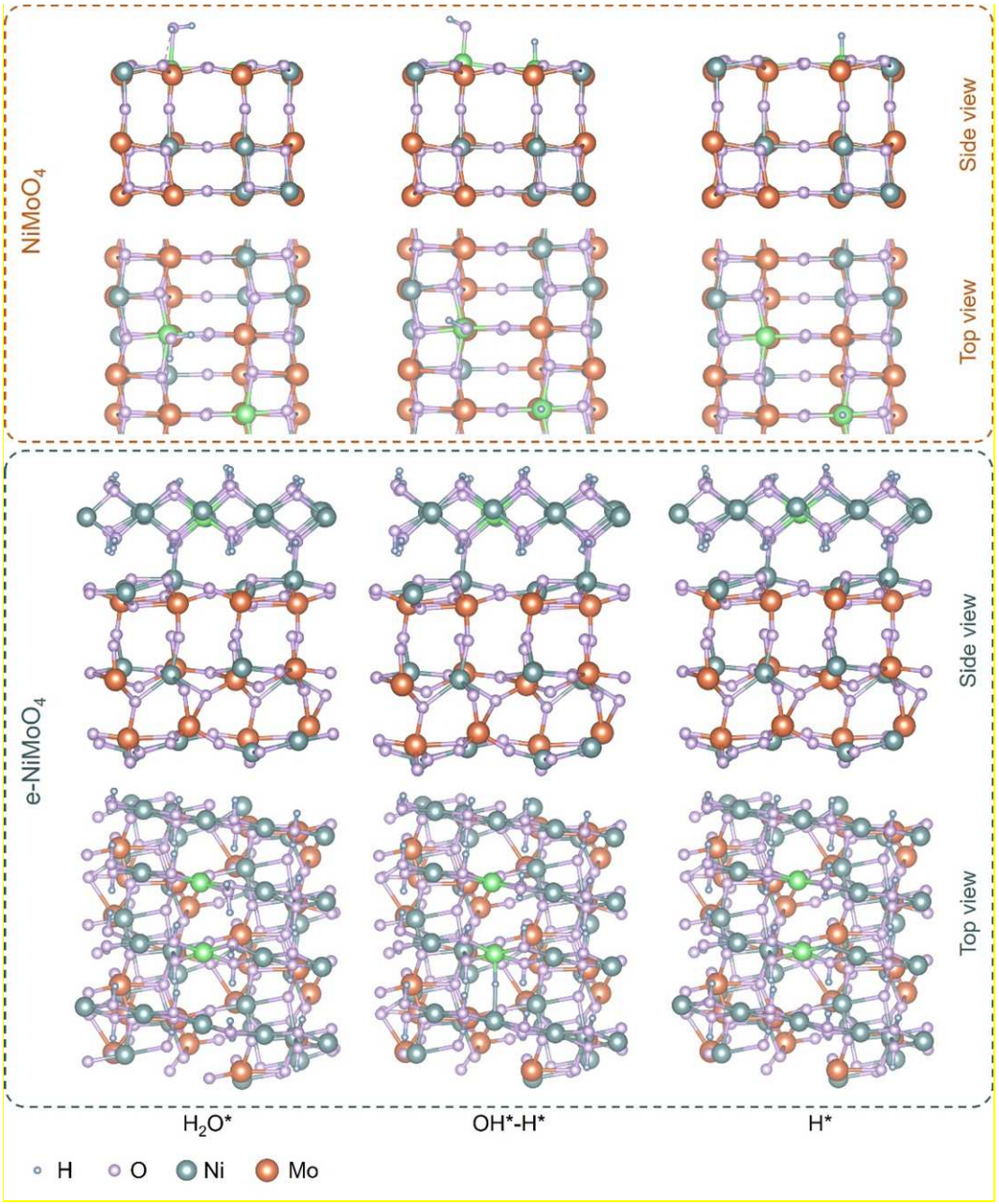

Supplementary Fig. 33 The theoretical models of different adsorption reaction groups on $NiMoO_4$ and e-$NiMoO_4$.

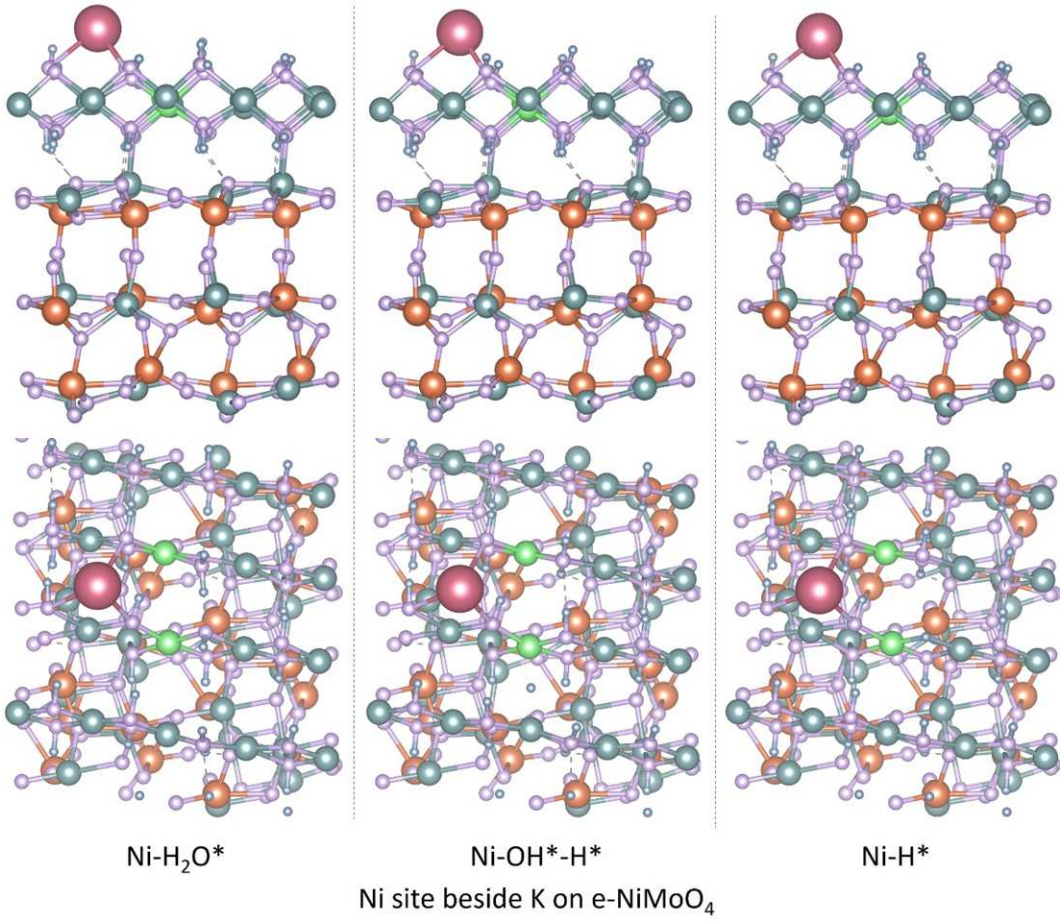

Supplementary Fig. 36 The theoretical models of different adsorption reaction groups on nickel site beside K ion on e-$NiMoO_4$.

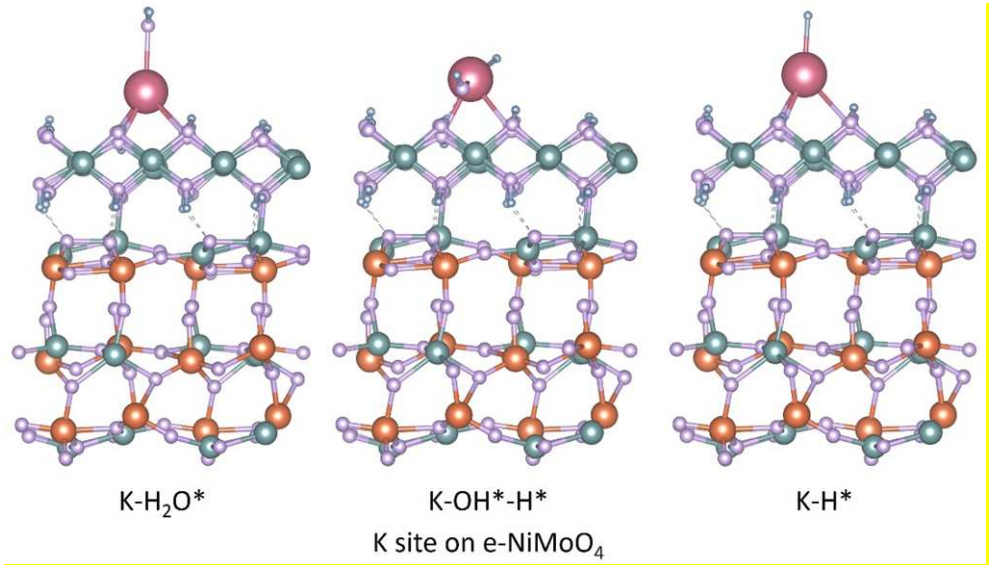

Supplementary Fig. 37. The theoretical models of different adsorption reaction groups on K sites on e-$NiMoO_4$.

"To further investigate the influence of K^+ ions on the reaction pathway of active sites, we analyzed their effect on e-$NiMoO_4$ (Supplementary Fig. 36-37). On the e-$NiMoO_4$ surface, the dissociation barrier of H_2O is 0.69 eV, primarily due to the slow cleavage of the O-H bond (Supplementary Fig. 38)[15, 42]. At Ni sites adjacent to K^+, the free energy barrier for the conversion of H_2O to OH-H reduction occurs because K^+ reduces the localization of charge density on H*, thereby facilitating faster OH*-H* decoupling. Additionally, K^+ lowers the Volmer barrier by rebalancing the equilibrium between H* adsorption and desorption."***(Page 12 in revised manuscript)***

Reference:

15. Cui W. G., *et al.* Insights into the pH effect on hydrogen electrocatalysis. *Chem. Soc. Rev.* **53**, 10253-10311 (2024).

42. Yang Y., *et al.* Electrocatalysis in alkaline media and alkaline membrane-based energy technologies. *Chem. Rev.* **122**, 6117-6321 (2022).

"To elucidate the detailed mechanism by which K^+ optimizes the alkaline HER pathway, we introduced K^+ ions near the active sites. On the e-$NiMoO_4$ surface, the dissociation barrier of H_2O is 0.69 eV, primarily due to the sluggish cleavage of the O-H bond[7]. The water activation barrier on K sites on e-$NiMoO_4$ remains excessively high, limiting its catalytic efficiency. In contrast, at the Ni site adjacent to K^+, the free energy barrier for the conversion of H_2O to OH-H is reduced, thereby facilitating faster OH*-H* decoupling[8]. Overall, the synergistic effect of K^+ is evident in the free energy landscape. While K^+ lowers the Volmer barrier, its primary role lies in rebalancing the H* adsorption–desorption equilibrium, which aligns well with experimental observations."***(Page 41 in revised supplementary materials)***

Supplementary Reference:

7. Cui W. G., *et al.* Insights into the ph effect on hydrogen electrocatalysis. *Chem. Soc. Rev.* **53**, 10253-10311 (2024).

Reviewer #3 (Comments to the Author): ==========

The goal of the authors is to introduce a dual-optimization strategy of dynamically constructing an epitaxial catalytic layer.The subject of the submitted paper carried out an interesting issue related to hydrogen production.Please find the attached file, which highlights in yellow or red color some possible misspellings or little grammatical suggestions. My principal concern is related to the computational issue.

Our response: Thank you very much for your affirmation of our work and good comments on manuscript. According to your comments, we made careful revisions to our manuscript and point-to-point response as below:

Specific comments:

Q1: *The introduction section contains many short sentences with many references. I suggest citing review papers and, additionally, discussing the results with data from the literature. For example, reference number 18 should be discussed in the results section instead of being cited in a generic paragraph in the introduction.*

Our response: Thank you for your constructive feedback. In response, we have revised the introduction to improve readability by consolidating short sentences and streamlining references. Additionally, we have incorporated relevant review papers to provide a more comprehensive background. Following your suggestion, we have moved the discussion of reference 18 to the results section, where it is now directly compared with our experimental data to provide a more contextualized analysis. These revisions enhance the clarity and logical flow of the manuscript. The corresponding revisions are as follows:

"The alkaline hydrogen evolution reaction (HER) holds significant potential for large-scale industrial hydrogen production. However, its efficiency is hindered by sluggish reaction kinetics, particularly in the initial water dissociation step (Volmer process, $H_2O \leftrightharpoons H + OH$) and the subsequent OH* desorption step ($OH^* + e^- \leftrightharpoons OH^-$), both of which introduce high energy barriers that limit overall alkaline water electrolysis performance[1-3]. Traditional approaches focus on optimizing the chemical and electronic structures of electrocatalytic materials to reduce the water dissociation activation energy and improve the stability of the catalyst surface[4-6]. Notably, the electrical double layer (EDL) structure at the catalyst-electrolyte interface, influenced by material properties and electrolyte characteristics,

contributes to the regulation of adsorption behavior, interfacial electric fields, and reactant concentration[7-9]. This enhances the availability of reactants at the interface, accelerates the transfer of reaction intermediates, and reduces the energy barriers for adsorbed reactants and intermediates. These findings provide valuable insights for designing efficient and stable alkaline electrolysis systems by achieving simultaneous optimization of the catalyst surface and electrolyte interface.

According to Koper's hemolytic and heterolytic models[10, 11], the proton-supplying ability of the electrolyte, specifically the concentration of reactants near the surface active sites, is a key descriptor in determining the overall catalytic activity for HER. During electrocatalytic reactions, the adsorption of various species on the electrode surface (including reactants, products, intermediates, and specifically adsorbed ions) plays a crucial role in governing the reaction's progress[12-15]. Traditionally, optimizing alkaline HER active sites has focused on regulating the adsorption and desorption barriers of H_2O/OH at the surface or within the inner Helmholtz plane[16-19]. However, changes in the concentration, arrangement, and configuration of solvent molecules and cations in the outer Helmholtz plane (OHP) within the EDL structure can also significantly influence the amount and adsorption energy of reaction intermediates at active sites [20-24]. These interfacial changes further impact proton-coupled electron transfer kinetics between interfacial solvent molecules and surface intermediates[25-27]. Therefore, mass transfer and local microenvironment regulation near the catalytic sites requires focusing on the OHP to optimize the electric field, ion distribution, and hydrogen bond network structure at the catalyst-electrolyte interface, ultimately enhancing the overall performance of alkaline HER."

(Page 12 in revised manuscript)

Reference:

2. Fairhurst A. R., Snyder J., Wang C., Strmcnik D., Stamenkovic V. R. Electrocatalysis: From planar surfaces to nanostructured interfaces. *Chem. Rev.* **125**, 1332-1419 (2025).

5. Quan L., Jiang H., Mei G., Sun Y., You B. Bifunctional electrocatalysts for overall and hybrid water splitting. *Chem. Rev.* **124**, 3694-3812 (2024).

6. Tüysüz H. Alkaline water electrolysis for green hydrogen production. *Acc. Chem. Res.*, 558-567 (2024).

9. Schott C. M., *et al.* How to assess and predict electrical double layer properties. Implications for electrocatalysis. *Chem. Rev.* **124**, 12391-12462 (2024).

15. Cui W. G., *et al.* Insights into the pH effect on hydrogen electrocatalysis. *Chem. Soc. Rev.* **53**, 10253-10311 (2024).

16. Chen C., *et al.* Local reaction environment in electrocatalysis. *Chem. Soc. Rev.* **53**, 2022-2055 (2024).

18. Levell Z., *et al.* Emerging atomistic modeling methods for heterogeneous electrocatalysis. *Chem. Rev.* **124**, 8620-8656 (2024).

Q2: *I am confident that synergy between experiment and theory is an important branch of research. However, both approaches must be discussed at the same high level, and the lack of information can make it difficult to interpret or reproduce both observations and, consequently, the correlation between both results and observation. Perhaps some computational details of information can be added to the supplementary material.*

i) The theoretical model does not show the symmetry used in the computational models, nor does it describe which surface direction of $NiMoO_4$ is related to the morphology shown in the micrographs. For example, see Figure 1.

Our response: We appreciate your valuable comments. The theoretical models and symmetry-related descriptions are now included in the supplementary materials. Regarding symmetry, the INCAR parameter settings are as follows (Supplementary **Table 5**). The space group of the slab model for $NiMoO_4$ is C2/M with the (220) facet, while the space group for $Ni(OH)_2$ is P-3M1 with the (001) facet. For $Ni(OH)_2$, the (100) facet is the growth direction, and the calculated (001) facet is consistent with HRTEM observations.

Supplementary Table 5. INCAR parameters.

	INCAR-Freq	INCAR-Relax	INCAR-TS
ALGO	Fast	Fast	Normal
ISPIN	2	2	2
IBRION	5	2	3
NSW	300	500	500
EDIFFG	-0.02	-0.02	-0.05
POTIM	0.015	0.1	-
ISIF	2	2	2
IVDW	11	11	11
ISYM	0	0	0
ENCUT	450	450	450

ISMEAR	0	0	0
SIGMA	0.05	0.05	0.05
EDIFF	1e-7	1e-5	1e-5
NELMIN	5	5	5
NELM	300	300	300
GGA	PE	PE	PE
LREAL	Auto	Auto	Auto
MAGMOM	NFREE = 2	40*2 24*2 120*0.1 33*0.1	40*4 24*2 121*0.1 34*0.1 1*0.

ii) Where is the adopted crystallographic information file (CIF) file?

Our response: Thanks for your comments. All CIF files used for the calculations, including those for the bulk and slab structures, along with the OUTCAR files generated from the VASP calculations, are provided.

iii) The calculation of Gibbs free energies is not clearly explained. Did harmonic calculation calculate it? How to obtain the TS parameter?

Our response: Thank you for your valuable feedback. In our study, the Gibbs free energy values were computed using the harmonic approximation, and we performed vibrational frequency calculations to obtain the zero-point energy and entropy contributions. The transition state (TS) parameters were determined using the climbing image nudged elastic band (CI-NEB) method, which allows for the identification of the transition state along the reaction path (Supplementary **Table 7**). We have now included a more detailed explanation of these computational procedures in the revised manuscript to clarify how the Gibbs free energies and TS parameters were obtained. The newly supplemented data are summarized below and have been added to the revised manuscript:

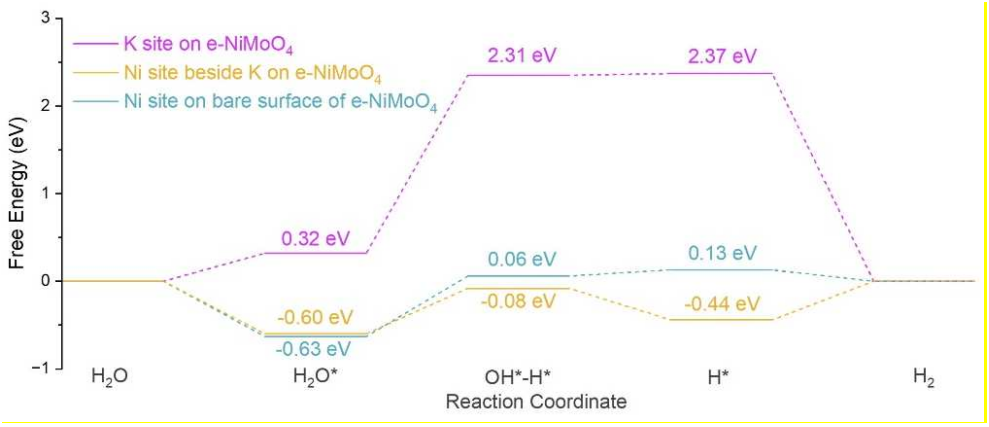

Supplementary Fig. 38. Free energy profile for the alkaline HER process on different sites on e-$NiMoO_4$.

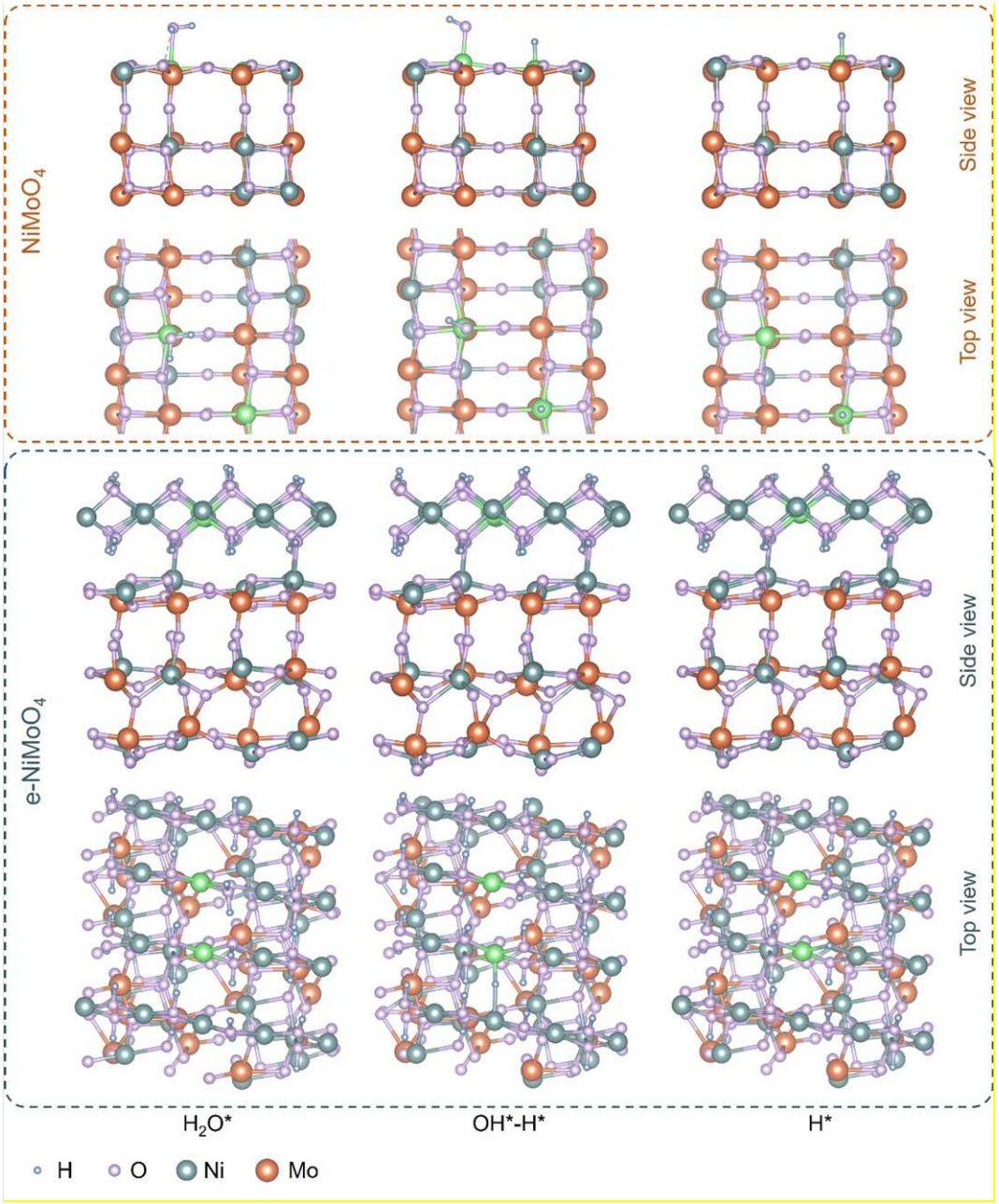

Supplementary Fig. 33 The theoretical models of different adsorption reaction groups on $NiMoO_4$ and e-$NiMoO_4$.

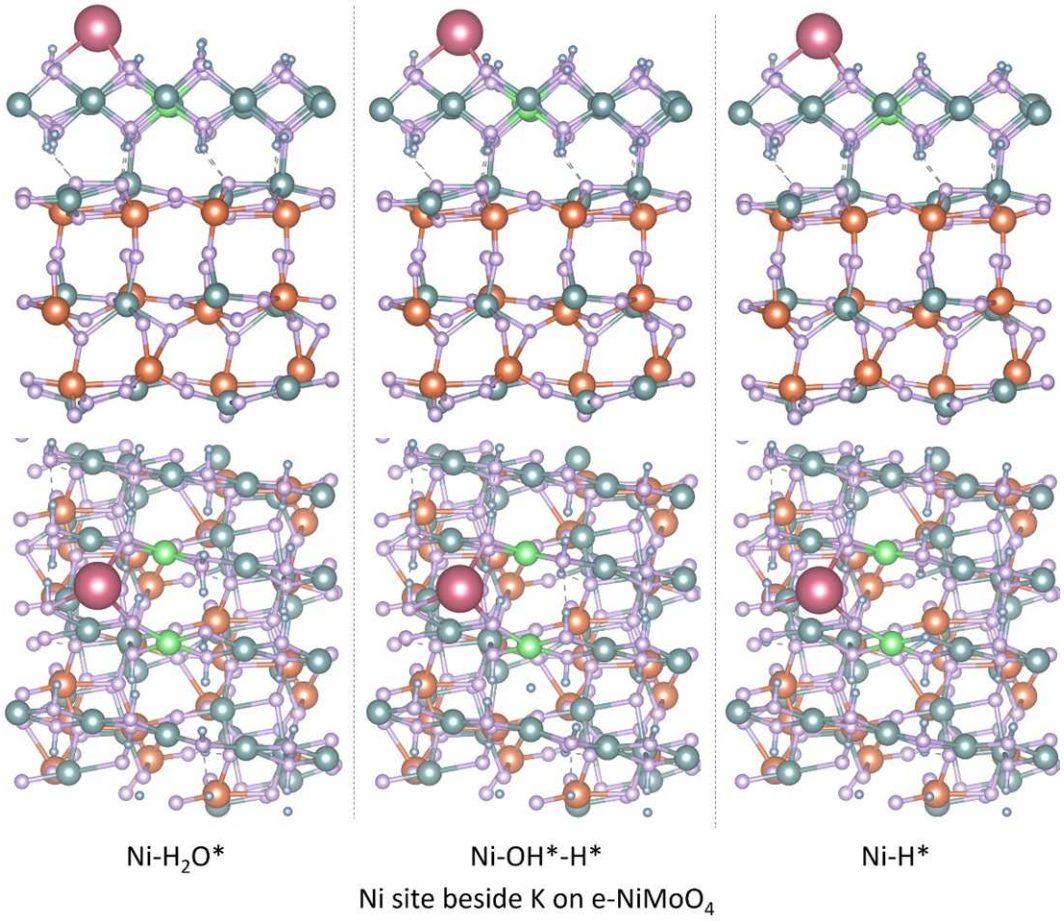

Supplementary Fig. 36 The theoretical models of different adsorption reaction groups on nickel site beside K ion on e-$NiMoO_4$.

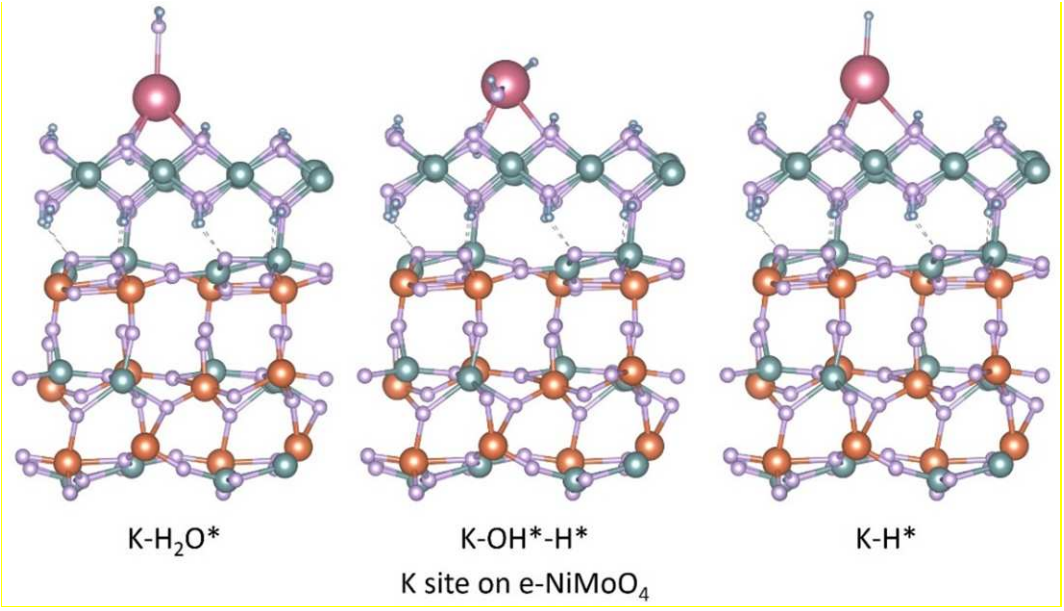

Supplementary Fig. 37. The theoretical models of different adsorption reaction groups on K sites on e-$NiMoO_4$.

Supplementary Table 7. The specific values of the zero-point energy (ZPE) and transition state (TS) for each reaction intermediate during the Gibbs free energy calculations.

$NiMoO_4$	$*H_2O$	*OH+*H	*H
ΔE_{ZPE}	0.7379	0.5920	0.2203
$T\Delta S$	0.1038	0.0003	0.0090
e-$NiMoO_4$	$*H_2O$	*OH+*H	*H
ΔE_{ZPE}	0.7222	0.6431	0.1685
$T\Delta S$	0.3702	0.1386	-0.0428
K site e-$NiMoO_4$	$*H_2O$	*OH+*H	*H
ΔE_{ZPE}	0.6777	0.4172	0.0960
$T\Delta S$	0.1443	0.1941	0.1288
Ni site besdie K	$*H_2O$	*OH+*H	*H
ΔE_{ZPE}	0.6667	0.6251	0.1643
$T\Delta S$	0.0912	0.0585	0.0132

"To further investigate the influence of K^+ ions on the reaction pathway of active sites, we analyzed their effect on e-$NiMoO_4$ (Supplementary Fig. 36-37). On the e-$NiMoO_4$ surface, the dissociation barrier of H_2O is 0.69 eV, primarily due to the slow cleavage of the O-H bond (Supplementary Fig. 38)[15, 42]. At Ni sites adjacent to K^+, the free energy barrier for the conversion of H_2O to OH-H reduction occurs because K^+ reduces the localization of charge density on H*, thereby facilitating faster OH*-H* decoupling. Additionally, K^+ lowers the Volmer barrier by rebalancing the equilibrium between H* adsorption and desorption."***(Page 12 in revised manuscript)***

Reference:

15. Cui W. G., *et al.* Insights into the pH effect on hydrogen electrocatalysis. *Chem. Soc. Rev.* **53**, 10253-10311 (2024).

42. Yang Y., *et al.* Electrocatalysis in alkaline media and alkaline membrane-based energy technologies. *Chem. Rev.* **122**, 6117-6321 (2022).

"To elucidate the detailed mechanism by which K^+ optimizes the alkaline HER pathway, we introduced K^+ ions near the active sites. On the e-$NiMoO_4$ surface, the dissociation barrier of H_2O is 0.69 eV, primarily due to the sluggish cleavage of the O-H bond[7]. The water activation barrier on K sites on e-$NiMoO_4$ remains excessively high, limiting its catalytic

efficiency. In contrast, at the Ni site adjacent to K^+, the free energy barrier for the conversion of H_2O to OH-H is reduced, thereby facilitating faster OH*-H* decoupling[8]. Overall, the synergistic effect of K^+ is evident in the free energy landscape. While K^+ lowers the Volmer barrier, its primary role lies in rebalancing the H* adsorption–desorption equilibrium, which aligns well with experimental observations."***(Page 41 in revised supplementary materials)***

Supplementary Reference:

7. Cui W. G., *et al.* Insights into the ph effect on hydrogen electrocatalysis. *Chem. Soc. Rev.* **53**, 10253-10311 (2024).

iv) Please, the DFT computational details section should be moved out of the characterization section.

Our response: Thank you for your suggestion. In the original manuscript, the theoretical calculation details were not included within the characterization section but were presented as a separate section of equal importance. We have revised the experimental section to ensure a clearer presentation of the theoretical methods, enhance the manuscript's logical structure, and minimize potential misunderstandings for readers.

"**DFT Computational details**

All the calculations are performed in the framework of the density functional theory with the projector augmented plane-wave method, as implemented in the Vienna ab initio simulation package. The exchange-correlation potential was treated by using a generalized gradient approximation (GGA) with the Perdew-Burke-Ernzerhof (PBE) parametrization[46]. The van der Waals correction of Grimme's DFT-D3 model was also adopted [47]. $NiMoO_4$ (110) was selected as the calculation model, lattice parameters were a = 15.3 Å, b = 12.9 Å, and c =30 Å. $Ni(OH)_2$ (001) was used to construct the heterojunction with NiMoO4 (110) , lattice parameters were a = 13.5 Å, b = 12.2 Å, and c =30 Å. The energy cutoff was set to be 450 eV. 2× 2× 1 Gamma k-point sampling is used for the Brillouin zone integration [48]. The energy criterion is set to 10^{-5} eV in iterative solution of the Kohn-Sham equation. A vacuum layer of 15 Å is added perpendicular to the sheet to avoid artificial interaction between periodic images. All the structures are relaxed until the residual forces on the atoms have declined to less than 0.01 eV/Å.

The free energy of hydroxyl adsorption on are defined as:

$$\Delta G_{OH} = G_{sur-OH} - G_{sur} - G_{OH^-}$$

where G_{sur-OH}, G_{OH}, and G_{sur} are the free energies of species adsorbed, hydroxyl species and clean surfaces, respectively. At equilibrium potential of HER:

$$G_{H_2O} = G_{OH^-} + \frac{1}{2}G_{H_2}$$

Thus,

$$\Delta G_{OH} = G_{sur-OH} - G_{sur} - G_{H_2O} + \frac{1}{2}G_{H2}$$

TS values are from previous report:

$$\Delta G_{OH} = E_{sur-OH} - E_{sur} - E_{H_2O} + \frac{1}{2}E_{H_2} + 0.29eV$$

The solvent induced polarization charge is calculated based on PWmat code with similar setup. Visualization of the atomic structures are made by using VESTA. Herein, four main steps in alkaline HER are considered: water adsorption and activation, H* intermediates formation, H_2 formation.

The Gibbs free energy (G) of each intermediate or product is given by

$$\Delta G = \Delta E + \Delta E_{ZPE} - T\Delta S$$

where ΔE is the quantum-chemical reaction energy directly obtained from DFT calculations; ΔE_{ZPE} and ΔS are the correction of zero-point energy and entropy, respectively, calculated from the vibrational frequencies; T is the temperature (298.15 K in this work); The computational hydrogen electrode (CHE) model proposed by Nørskov [49]."***(Pages 18~19 in revised manuscript)***

Reference:

46. Perdew J. P., Burke K., Ernzerhof M. Generalized gradient approximation made simple. *Phys. Rev. Lett.* **77**, 3865-3868 (1996).
47. Grimme S., Antony J., Ehrlich S., Krieg H. A consistent and accurate ab initio parametrization of density functional dispersion correction (DFT-D) for the 94 elements H-Pu. *J. Chem. Phys.* **132**, 154104 (2010).
48. Monkhorst H. J., Pack J. D. Special points for brillouin-zone integrations. *Phys. Rev. B* **13**, 5188-5192 (1976).
49. Norskov J. K., *et al.* Origin of the overpotential for oxygen reduction at a fuel-cell cathode. *J. Phys. Chem. B* **108**, 17886-17892 (2004).

v) What is the state of the art on $NiMoO_4$?

Our response: We appreciate your comments. Significant progress has been made in the study of $NiMoO_4$ as an electrocatalyst for water splitting, with a primary focus on nanoscale structural modulation, electronic structure optimization, and composite material design. Research has demonstrated that tailoring the nanostructure of $NiMoO_4$ (e.g., *Energy Environ. Sci.*, **2024**, 17, 332; *Appl. Catal. B: Environ.*, **2025**, 366, 125024) enhances the specific surface area and exposes more active sites, thereby improving catalytic activity. Additionally, elemental doping (e.g. *Nat. Commun.* **2021**, 12, 5960; *Appl. Catal. B: Environ.*, **2024**, 347, 123805; *Adv. Funct. Mater.*, **2023**, 33, 2210855.) and the construction of heterojunctions (e.g., *Nat. Commun.* **2024**, 15, 8293; *Adv. Energy Mater.*, **2024**, 14, 2304546; *Adv. Energy Mater.*, **2021**, 11, 2101324) effectively optimize the electronic structure, reducing the HER energy barrier and further enhancing catalytic performance. In this study, we designed an epitaxial $Ni(OH)_2$ dendritic layer on $NiMoO_4$ and regulated the interfacial electrochemical behavior through surface electrostatic microenvironment modulation, ultimately improving catalytic activity. These findings provide new insights into the design of $NiMoO_4$-based catalysts.

vi) A lack of references has been noticed throughout the work. Among them, COMSOL and more….

Our response: We sincerely appreciate your valuable suggestions for improving the comprehensiveness of our study. In the revised manuscript, we have incorporated additional references to strengthen the discussion on the research background, experimental methods, and theoretical calculations. For instance, in the computational modeling section, we have added citations related to COMSOL Multiphysics to clarify the basis of our calculations and reference prior studies. Furthermore, we have included recent research findings on catalytic performance analysis, interfacial regulation mechanisms, and material stability to enhance the theoretical and experimental support for our work.

COMSOL simulation details

Using the COMSOL Multiphysics finite element solver (https://www.comsol.com/), we simulated the free electron density on the electrode, as well as the electric field and potassium ion density near the electrode. The "Electric Currents" module was employed to solve for the free electron density on the electrode under a specific electrode bias potential[50, 51]. The electric field E was calculated as the negative gradient of the potential V, given by $E = -\nabla V$.

$$\nabla \cdot \boldsymbol{J} = Q_{j,v}$$

$$\boldsymbol{J} = \sigma \boldsymbol{E} + \frac{\partial \boldsymbol{D}}{\partial t} + J_e$$

The diffusion layer consists of potassium ions that freely diffuse within the electrolyte. A concentration gradient is formed toward and away from the electrode surface through the tracking of charged particles.

$$\frac{d}{dt}\left(m_p \frac{d\boldsymbol{q}}{dt}\right) = F_t$$

Combine the "Electrostatics" and "Diluted Species Transport" modules to solve for the potassium ion density in the electric double layer [52, 53].

$$\frac{\partial c_i}{\partial t} + \nabla \cdot \boldsymbol{j}_i + \boldsymbol{u} \cdot \nabla c_i = R_i$$

$$J_i = -D_i \nabla c_i - z_i u_{m,j} F c_i \nabla v$$

(Pages 20~21 in revised manuscript)

Reference:

50. Gomez-Tames J., Gonzalez J., Yu W. Influence of different geometric representations of the volume conductor on nerve activation during electrical stimulation. *Comput. Math. Methods Med.* **2014**, 489240 (2014).
51. Joucla S., Gliere A., Yvert B. Current approaches to model extracellular electrical neural microstimulation. *Front. Comput. Neurosci.* **8**, 13 (2014).
52. Banerjee T., Ghoshal S., Bhattacharya B. B. Comsol-based design and validation of dilution algorithm with continuous-flow lab-on-chip. *INAE Lett.* **2**, 55-63 (2017).
53. Adam T., Hashim U. Comsol multiphysics simulation in biomedical engineering. *Adv. Mater. Res.* **832**, 511-516 (2013).

vii) Where is the CIF file for each adopted model?

Our response: Thank you for your comments. We have provided all CIF files used in the calculations, including those for the bulk and slab structures, as well as the OUTCAR files generated from the VASP calculations.

viii) The total and projected density of states does not bring relevant pieces of information. I suggest COHP analysis and a more detailed discussion:
https://pubs.acs.org/doi/10.1021/jp202489s<https://urldefense.com/v3/__https://pubs.acs.org

/doi/10.1021/jp202489s__;!!Nmw4Hv0!w-FgPFRH6MlAz7q5RgILA6f8fhiNiTBsuQAtOFfCAlwNoRwC2DBGUfFFyMDa9nm7KmplyvqYdeAEir96YypK9PtYiGmKnBHr$>

Our response: We agree with your suggestion. We have performed a Crystal Orbital Hamilton Population (COHP) analysis and provided the pCOHP and ICOHP values for the OH bond after H_2O adsorption on the surfaces of $NiMoO_4$ and e-$NiMoO_4$ (Supplementary **Fig. 32**). This analysis offers a more detailed understanding of the atomic interactions, particularly at the catalyst-electrolyte interface. e-$NiMoO_4$ exhibits a lower ICOHP compared to $NiMoO_4$, indicating weaker bonding interactions between the catalyst and the adsorbed species, which enhances the adsorption and activation of water molecules, thereby improving its HER activity. The newly supplemented data are summarized below and have been added to the revised manuscript:

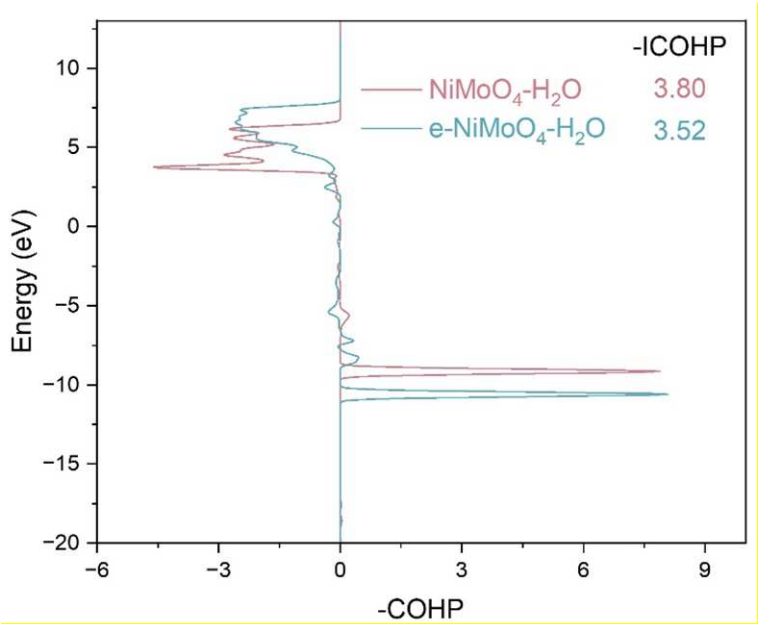

Supplementary Fig. 32. Crystal orbital Hamilton population (COHP) analysis of the O-H bond in the adsorbed OH* for $NiMoO_4$ and e-$NiMoO_4$.

Q3: *The water-splitting mechanism and hydrogen evolution reaction deserve to be elucidated. Much of this can be extracted by quantum mechanical methods..*

Our response: We acknowledge and appreciate your comments. To elucidate the rate-determining step of the reaction, we investigated the kinetic energy barriers. Transition state energy analysis revealed significant differences in the dissociation pathway of H_2O into OH^-

and H* at the nickel site (bare surface of e-$NiMoO_4$), nickel site (beside K on e-$NiMoO_4$), and the K^+ adsorption site (K site on e-$NiMoO_4$) during alkalin HER (Supplementary **Fig. 40-43**). On the nickel site of the bare e-$NiMoO_4$ surface, the transition state energy for H_2O dissociation (TS = 0.90 eV) is relatively low, indicating a lower O–H bond cleavage barrier and faster reaction kinetics. The final state energy (0.73 eV) further confirms the high stability of the dissociated OH^- and H* intermediates, facilitating subsequent reaction steps. In contrast, at the K site, the transition state energy increases significantly (TS = 3.93 eV), with a final state energy of 2.55 eV, much higher than that at the nickel site. This suggests that the stability of the dissociated OH^--H* intermediate is considerably lower, potentially requiring additional energy input to sustain the reaction. Interestingly, at the nickel site adjacent to K^+, the transition state energy barrier is the lowest (0.70 eV). This indicates that the presence of K^+ further reduces the HER energy barrier at the nickel site, likely enhancing its catalytic activity through electronic effects or local environmental modulation. As a result, K^+ promotes O–H bond cleavage and ultimately improves HER efficiency under alkaline conditions.

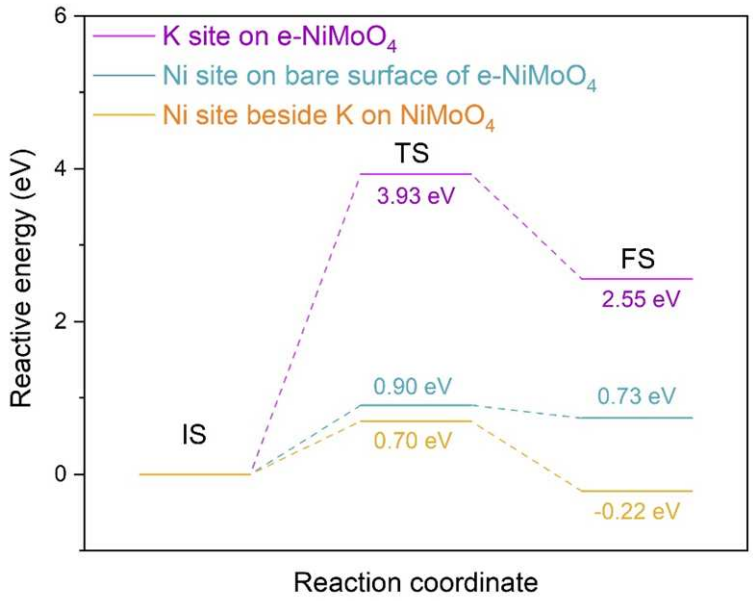

Supplementary Fig. 42. Transition state analysis at different active sites.

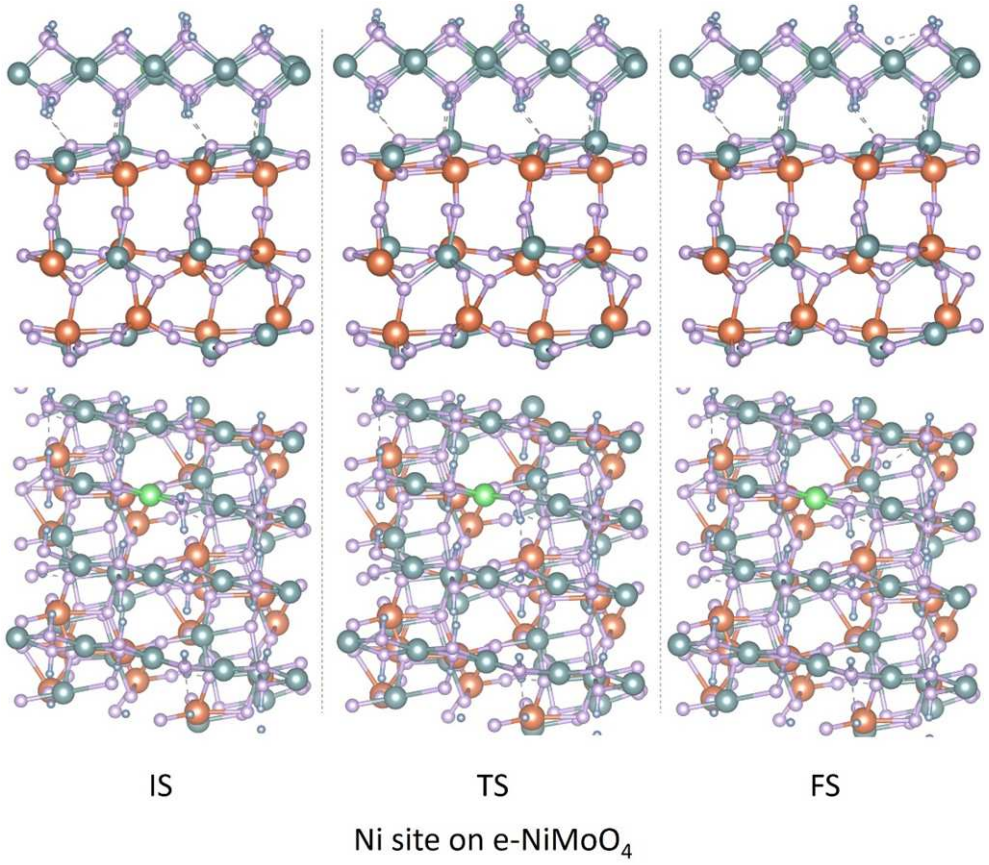

Supplementary Fig. 39 The theoretical models of different reaction state on nickel sites of e-$NiMoO_4$.

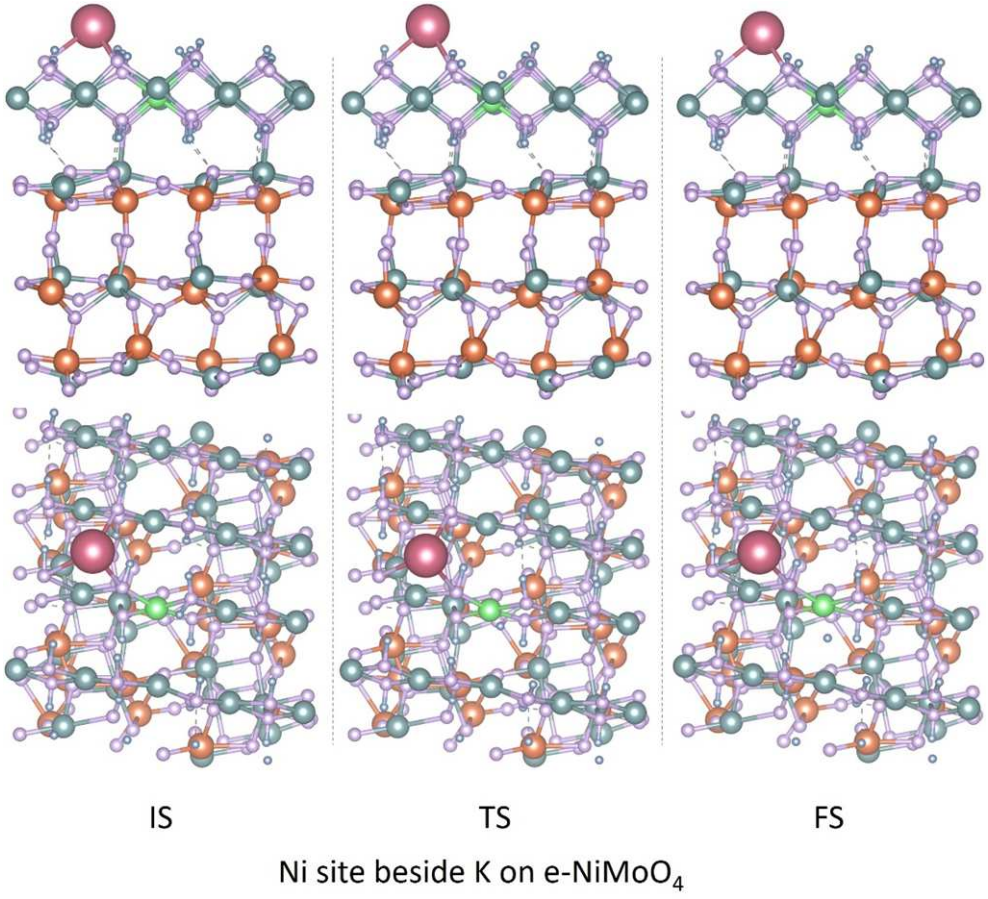

Supplementary Fig. 40 The theoretical models of different reaction state on nickel sites beside K of e-$NiMoO_4$.

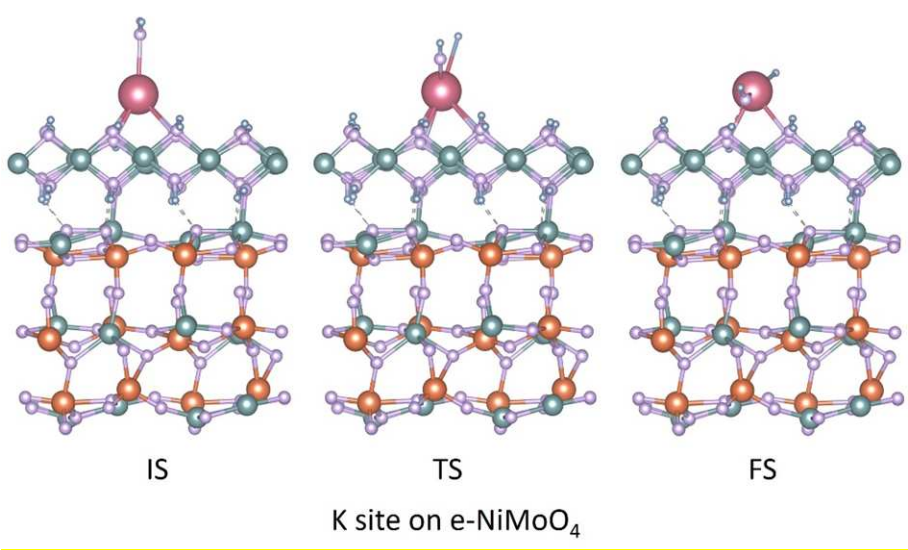

Supplementary Fig. 41 The theoretical models of different reaction state on K sites of e-$NiMoO_4$.

Supplementary Table 7. The specific values of the zero-point energy (ZPE) and transition state (TS) for each reaction intermediate during the Gibbs free energy calculations.

$NiMoO_4$	$*H_2O$	*OH+*H	*H
ΔE_{ZPE}	0.7379	0.5920	0.2203
$T\Delta S$	0.1038	0.0003	0.0090
e-$NiMoO_4$	$*H_2O$	*OH+*H	*H
ΔE_{ZPE}	0.7222	0.6431	0.1685
$T\Delta S$	0.3702	0.1386	-0.0428
K site e-$NiMoO_4$	$*H_2O$	*OH+*H	*H
ΔE_{ZPE}	0.6777	0.4172	0.0960
$T\Delta S$	0.1443	0.1941	0.1288
Ni site besdie K	$*H_2O$	*OH+*H	*H
ΔE_{ZPE}	0.6667	0.6251	0.1643
$T\Delta S$	0.0912	0.0585	0.0132

"At Ni sites adjacent to K^+, the transition state energy barrier is the lowest (0.70 eV), with a final state energy of -0.22 eV, indicating that K^+ further reduces the HER energy barrier at these sites (Supplementary Fig. 40-43, Table 8)."***(Pages 12 in revised manuscript)***

"Transition state energy analysis revealed significant differences in the dissociation pathway of H_2O into OH^- and H* at the nickel site (bare surface of e-$NiMoO_4$), nickel site (beside K on e-$NiMoO_4$), and the K^+ adsorption site (K site on e-$NiMoO_4$) during alkalin HER. On the nickel site of the bare e-$NiMoO_4$ surface, the transition state energy for H_2O dissociation (TS = 0.90 eV) is relatively low, indicating a lower O–H bond cleavage barrier and faster reaction kinetics[8]. The final state energy (0.73 eV) further confirms the high stability of the dissociated OH^- and H* intermediates, facilitating subsequent reaction steps. In contrast, at the K site, the transition state energy increases significantly (TS = 3.93 eV), with a final state energy of 2.55 eV, much higher than that at the nickel site. This suggests that the stability of the dissociated OH^--H* intermediate is considerably lower, potentially requiring additional energy input to sustain the reaction. Furthermore, at the nickel site adjacent to K^+, the transition state energy barrier is the lowest (0.70 eV), and the final state energy is -0.22 eV. This indicates that the presence of K^+ further reduces the HER energy barrier at the nickel site, enhancing its catalytic activity."***(Page 45 in revised supplementary materials)***

Supplementary Reference:

8. Yang Y., *et al.* Electrocatalysis in alkaline media and alkaline membrane-based energy technologies. *Chem. Rev.* **122**, 6117-6321 (2022).